IN SILICO SCREENING OF THE APPROVED DRUGS, PEPTIDOMIMETICS AND DESIGNING OF NEW PEPTIDES AGAINST AXL-GAS6 TARGET

İLAYDA TOLU

MAY 2022

IN SILICO SCREENING OF THE APPROVED DRUGS, PEPTIDOMIMETICS AND DESIGNING OF NEW PEPTIDES AGAINST AXL-GAS6 TARGET

A THESIS SUBMITTED TO THE
GRADUATE SCHOOL
OF
BAHCESEHIR UNIVERSITY

İLAYDA TOLU

IN PARTIAL FULFILLMENT OF THE REQUIREMENTS

FOR

THE DEGREE OF

NEUROSCIENCE DEPARTMENT

MAY 2022

T.C.
BAHCESEHIR UNIVERSITY
GRADUATE SCHOOL

MASTER THESIS APPROVAL FORM

Program Name:	Neuroscience Program
Student's Name and Surname:	İlayda Tolu
Name Of the Thesis:	In Silico Screening of the Approved Drugs, Peptidomimetics and Designing of New Peptides Against Axl-Gas6 Target
Thesis Defence Date:	31 Mayıs 2022

This thesis has been approved by the Graduate School and has fulfilled the necessary conditions as a master's thesis.

Prof. Dr. Ahmet ÖNCÜ
Institute Director

This thesis was read by us, quality and content as a master's thesis have been seen and accepted as sufficient.

	Title/Name	**Signature**
Thesis Advisor's	Prof. Dr. Serdar Durdağı	
Member's	Assist. Prof. Dr. Berna Doğan	
Member's	Assoc. Prof. Dr. Mert Gür	

I hereby declare that all information in this document has been obtained and presented in accordance with academic rules and ethical conduct. I also declare that, as required by these rules and conduct, I have fully cited and referenced all material and results that are not original to this work.

Name, Last Name: İlayda TOLU

Signature:

ABSTRACT

IN SILICO SCREENING OF THE APPROVED DRUGS, PEPTIDOMIMETICS AND DESIGNING OF NEW PEPTIDES AGAINST AXL-GAS6 TARGET

Tolu, İlayda
Master's Program in Neuroscience
Supervisor: Prof. Dr. Serdar Durdağı

May 2022, 70 Pages

Axl is one of the members of the TK family. It is mainly responsible for cell proliferation and migration. Axl is also found related to cancer cell metastasis and angiogenesis. Gas6 is the natural ligand of Axl. It binds on the cell membrane receptors and initiates signalling. The aim of this study is to investigate new therapeutic molecules against Axl-Gas6 target by screening approved drugs and compounds in clinical investigation and peptidomimetic databases. Based on the binary cancer QSAR model prediction scores 1341 peptidomimetics and 1089 compounds in FDA approved ligand library were further studied on molecular docking simulations. In docking, two different binding sites and three different systems have been studied. Based on docking studies, top 10 compounds for each system were studied for short molecular dynamics (MD) simulations. Later, long MD simulations for the top-5 molecules were studied. Average MM/GBSA was calculated. As a result, G842-0689 and F723-0087 have higher negative binding energies than reference molecules on the site 1 on the A chain. Furthermore, 10 peptides were designed. Ten peptides were studied for molecular docking simulations on site 2 and on the C chain only. After docking studies, short MD simulations were performed. Later, long MD simulations were conducted. The results indicate that these small molecules on peptidomimetic and FDA databases and ten designed peptides can be considered as good candidates as inhibitors of the Axl-Gas6 complex in the treatment of kidney cancer. However, these in silico results must be validated by in vitro experiments.

Key Words: Axl-Gas6, Peptide Design, Computer Aided Drug Design, molecular docking, MD Simulations.

ÖZ

ONAYLI İLAÇLARIN VE PEPTİDOMİMETİK LİGANTLARIN AXL-GAS6 HEDEFİNE KARŞI İN SİLİKO TARANMASI VE BU HEDEFE YÖNELİK YENİ PEPTİTLERİN TASARLANMASI

Tolu, İlayda

Sinirbilim Yüksek Lisans Programı

Tez Danışmanı: Prof. Dr. Serdar Durdağı

Mayıs 2022, 70 Sayfa

Axl tirosin kinaz ailesinin bir üyesidir. Hücre çoğalması ve göçünden mesuldür. Gas6, Axl hedefinin ligandıdır. Hücre zarı reseptörlerine bağlanarak hücre içi sinyalin başlatılmasını sağlar. Bu çalışmanın amacı, FDA onaylı ilaçları ve peptidomimetik veri tabanlarını tarayarak Axl-Gas6 hedeflerine karşı yeni moleküllerin araştırılmasıdır. İkili kanser QSAR modeli tahmin skorlarına dayanarak 1341 peptidomimetik ve 1089 onaylı veya klinik faz çalışmalarında yer alan moleküle moleküler yerleştirme simülasyonları yapıldı. Yerleştirmede, iki farklı bağlanma bölgesi, ve Axl-Gas6 protein kompleksinin yalnız ve birlikte formları ile üç farklı sistem çalışılmıştır. Yerleştirme çalışmalarında, her sistemden en iyi 10 bileşik ile kısa (50 ns) moleküler dinamik simülasyonlar yapılmıştır. Daha sonra en iyi ilk 5 molekül ile uzun MD simülasyonlar yapılmıştır. MD simülasyonlardan elde edilen trajektöriler için ortalama bağlanma enerjileri (MM/GBSA) hesaplanmıştır. Sonuç olarak, birinci bağlanma bölgesinde, A zincirinde G842-0689 ve F723-0087 moleküllerinin, referans moleküllerden daha negatif bağlanma enerjilerine sahip olduğu hesaplanmıştır. AC zincirlerinde birinci bölgede Saquinavir ve Gonadorelin referans moleküllerden daha negatif skora sahip olduğu bulunmuştur. Ayrıca 10 adet peptit tasarımı yapılmıştır. İkinci bölgede yalnızca C zincirinde incelenen 10 peptit için moleküler kenetleme ve MD simülasyonlar yapılmıştır. Yerleştirme çalışmalarından sonra, kısa MD ve uzun MD simülasyonları gerçekleştirilmiştir. Elde edilen sonuçlarda peptitlerin simülasyonlar boyunca ikincil yapısının koruduğu ve bağlanma enerjilerin -100.00

kkal/mol'den daha düşük değerlere sahip olduğu hesaplanmıştır. Elde edilen sonuçlar kullanılan veri tabanlarındaki bu küçük moleküllerin ve tasarlanan 10 peptidin böbrek kanseri tedavisinde önemli rolü olan Axl-Gas6 kompleksinin inhibitör adayları olarak düşünülebileceğini göstermektedir. Ancak in vitro deneyler ile bu in siliko sonuçların validasyonun yapılması gereklidir.

Anahtar Kelimeler: Axl-Gas6, Peptit Dizaynı, Bilgisayar Destekli İlaç Tasarımı, Moleküler Kenetlenme, MD Simülasyonlar

Dedicating to people who support me,

ACKNOWLEDGEMENTS

It was a long and exhausted journey for me, but there were people who stand next to me. I want to thank them. First, I want to thank my family for their eternity support. Then, I want to thank Prof. Dr. Serdar Durdağı for his leading. Later, all the lab members and mostly Dr. İsmail Erol helped me a lot. All the time, they were there for me and my life partner Ege Mert Tan, thank you for all your emotional support and believe in me. I am very glad that I have all of you by my side.

TABLE OF CONTENTS

LIST OF TABLES

TABLES

LIST OF FIGURES

FIGURES

LIST OF ABBREVIATIONS

2D	2-dimensional
3D	3-dimensional
3D-QSAR	3-dimensional Quantitative Structure Activity Relationships
AML	Adult Acute Myeloid Leukaemia
CADD	Computer Aided Drug Design
CML	Chronic myelogenous Leukaemia
EGF	Epidermal Growth Factor
FNIII	Fibronectin III
Gla	γ-carboxyglutamate
HTVS	High Through Virtual Screening
IFD	Induced-fit Docking
IG	Immunoglobulin
kDa	Kilodalton
LBDD	Ligand Based Drug Design

LG	Laminin -like Protein
MD	Molecular Dynamics
MM/PBSA	Molecular Mechanics Poisson-Boltzmann Surface Area
MM/GBSA	Molecular Mechanics Generalized Born Surface Area
NK	Natural Killer
NMR	Nuclear Magnetic Resonance
PCR	Polymerase Chain Reaction
QM	Quantum Mechanics
RTK	Receptor Tyrosine Kinase
RT-PCR	Real-Time Polymerase Chain Reaction
SBDD	Structure-Based Drug Design
SP	Standard Precision
TAM	Tyro3-Axl-MerTK
VMD	Visual Molecular Dynamics
XP	Extra Precision
TK	Tyrosine Kinase

Chapter 1

Introduction

Cancer was a disease discovered centuries ago, and still, no life-saving treatment has been discovered. Many treatments were studied, like chemotherapy, surgery, radiation therapy, targeted therapy, immunotherapy, hormone therapy, and stem cell transplant.

Cancer can be caused by various factors, including overexpression, aberrant protein function, and a variety of other factors. Tyro3-Axl-MerTK (TAM) receptor genes are proto-oncogenes, which explains why they play an essential role in cancer formation and spread. Axl, Tyro3, and MerTK are members of the TAM family. They are genetically or structurally related. The proteins in the family have three domains in general. Extracellular domain, transmembrane (TM) domain, and intracellular (tyrosine kinase) domain are the three types of domains (Vouri and Hafizi, 2017).

In glioblastoma cells, Axl expression lacking kinase domain activity causes a reduction in motility, alterations in cell shape, and a loss of cell-to-cell communication (Vajkoczy et al., 2006). TAM receptors recognize apoptotic cells in macrophages. Protein S is a TAM ligand that stimulates apoptotic cell phagocytosis. Gas6, another TAM family ligand, increases macrophage absorption of phosphatidylserine (PS) liposomes. It is found that Axl inhibits macrophage uptake (Ishimoto et al., 2000; Anderson et al., 2003).

The “Literature Review” section summarizes the cancer and TAM receptors to highlight the importance of this study and its results. In the Methodology section, the protocols used are mentioned in detail. The “Findings” shows the calculations and analyses the data obtained from the applied in silico experiments. Lastly, the findings are detailed and discussed in the “Discussion and Conclusions” sections.

Chapter 2

Literature Review

2.1 Receptor Tyrosine Kinase

RTK (Receptor Tyrosine Kinase) harbours nearly twenty different protein families with a similar structure or gene sequence. They all have three main domains: extracellular, transmembrane, and intracellular domains. The main aim of the RTKs is the regulation of multicellular processes like cell to cell recognition, cell migration, differentiation, growth, adhesion and motility (Robinson, Wu and Lin, 2000). RTK has been related to many diseases like cancer and diabetes. RTKs are the prototypes of the oncogenes.

The catalytic domain of the Tyrosine kinases has been conserved throughout the generations and species (Hangs and Quinn, 1991). The extracellular part of the RTKs shows some similar contents like fibronectin-like domains, immunoglobulin-like domains, and cysteine-rich regions. When the ligand comes and binds on the extracellular part of the protein, a structural change occurs, and the receptor dimerizes to be more stable (Heldin, 1995). The transmembrane part of the protein anchors the protein in the cell membrane and usually gives the α-helical structure. In mutation studies on this region showed that mutations occur in the transmembrane region of the TKs to activate the receptor in the ligand-independent way.

2.1.1 TAM Receptors

TAM family is one of the members of the RTKs family. Generally, there are three domains of the proteins in the family: Extracellular domain, transmembrane domain, and intracellular (tyrosine kinase) domain. The tyrosine kinase activity is found on the intracellular part of the protein (Vouri and Hafizi, 2017). They are getting signals from outside and transmit it inside the cell. The two immunoglobulin (IG)-like domains and two fibronectin III (FNIII) domains are found on the extracellular part of the protein. Those domains are responsible for cell to cell adhesion and neuronal cell

adhesion (Yamagata, Sanes and Weiner, 2003). On the other part of the RTK, FNIII and IGs are not found together, except Tie (Tie1) and Tek (Tie2) receptors. For example, VEGF, PDGF, and FGF have IG domains, while Insulin and Epinephrin have only the FNIII domain.

The gene sequences are similar in TAM receptors, and it is in between 3 to 5 kb (O'bryan et al., 1991; Mark et al., 1994). In the TAM family, Tyro-3 and Axl have the most common similar genomic structure because both have the same exon number, 20 (Lewis et al., 1996) and MerTK has 19 exons (Linger et al., 2008). On the other hand, Axl and MerTK have similarities in the genomic sequence of the tyrosine kinase domain (Robinson, Wu and Lin, 2000). The extracellular part of the TAM family has approximately thirty-three percent identical, fifty-five percent similar amino acid sequences, while the intracellular part has almost fifty-five percent sequence identity and seventy-four percent similarity. The protein Tyro-3 has 890, Axl has 894, and MerTK protein has 999 amino acid residues. After translation of the proteins, there are some posttranslational modifications like glycosylation, phosphorylation, and ubiquitination. Therefore, the size of the proteins is in the range of 100-140 kDa for Axl; and 165-205 kDa for Tyro-3 (O'Bryan et al., 1991; Valverde, 2005; Sather et al., 2007).

2.1.2 Discovery of TAM Receptors

In the 1990s, all members were cloned from different species, and they were all named differently. In 1988, Axl was identified in two patients with CML (Chronic Myelogenous Leukemia) (Liu, Hjelle and Bishop, 1988) and chronic myeloproliferative disorder. The genes identified as Axl which means uncontrolled in Greek (O'bryan et al., 1991). The other team named the gene as UFO describes the unknown function. In 1991, thirteen PCR fragments were identified with the specific tyrosine kinase domain and named as Tyro-1 to 13 (Lai and Lemke, 1991). Then, it was found that Tyro-7 is the gene named as Axl or UFO before. Tyro-12 has the same gene as the Mer, and Tyro-3 becomes the TAM family's third member (Linger et al., 2008).

2.1.3 Expression Patterns of TAM

Axl, Tyro-3, and Mer are expressed in plenty of tissues and cells. They are expressed in the same tissues and cells as well as in the same cells. For example, Tyro-3 is uniquely found on the nervous system, but also it may be found on the ovaries, testis, breast, kidney, macrophages, platelets, and retina (Mark et al., 1994; Angelillo-Scherrer et al., 2001; Katagiri et al., 2001; Lu and Lemke, 2001; Prasad et al., 2006). Axl is expressed all over the hippocampus, cerebellum (Bellosta et al., 1995), macrophages, platelets, heart, liver, kidney, and testis (Andreas Neubauer et al., 1994; Anne Angelillo-Scherrer et al., 2001). On the other hand, Mer is expressed in dendritic cells, macrophages, NK cells, and platelets (Anne Angelillo-Scherrer et al., 2001; Behrens et al., 2003). Mer is also expressed in ovaries, testis, kidneys, liver, and retina (Prasad et al., 2006).

2.1.4 Function of TAM

There had been several knockout experiments for the TAM family during embryogenesis. (Lai and Lemke, 1991; Crosier et al., 1996). Single, double, or even triple knockouts showed no defects in the development of the embryo. Therefore, TAM receptors are not essential proteins at the embryogenesis (Lu et al., 1999; Lu and Lemke, 2001; Lemke and Lu, 2003); however, in adult mice, knockout experiments showed different phenotypes in different tissues. The function of the receptors depends on the ligand, cell type, and microenvironment (Linger et al., 2008). In the knockout experiments of TAM receptors, it is concluded that autoimmune diseases like rheumatoid arthritis and lupus occur (Cohen et al., 2002; Lemke and Lu, 2003). Mer protein knockouts showed an increment in sensitivity for autoimmunity (Scott et al., 2001). As a result of the TAM receptor loss in the dendritic cells, apoptotic cells accumulate, and tissue necrosis occurs (Lu and Lemke, 2001). The phosphatidylserine (PS) is located on the apoptotic cells. They have been recognized by several PS receptors or indirectly via TAM receptor ligand Gas6 or Protein S (Nakano et al., 1997; Anderson et al., 2003). TAM receptors in the macrophages help to recognize the apoptotic cells. Protein S is a ligand for TAM family and also responsible for

stimulating the phagocytosis of apoptotic cells (Anderson et al., 2003). The other ligand of the TAM family is Gas6 which stimulates the macrophage uptake of PS liposomes. It is found that Axl blocks macrophage uptake (Ishimoto et al., 2000). Also, in another study, soluble Mer protein inhibits the macrophages of the apoptotic cells (Sather et al., 2007). Mer protein does not bind on the apoptotic cells but has a role in changing the shape of the cell during the apoptotic cell engulfment (Scott et al., 2001; Cohen et al., 2002; Guttridge et al., 2002; Hu et al., 2004; Todt, Hu and Curtis, 2004). The clearance of the apoptotic cells in the environment depends on the TAM receptor is mediated by the cell and organ type. Seitz et al. concluded that Mer has a role in macrophages clearance, and Axl, Tyro-3 mediates mainly clearance of apoptotic cells in the dendritic cells (Seitz et al., 2007).

2.1.5 Ligands of TAM

In 1995, Gas6, a vitamin K-dependent protein, was discovered as the ligand of the Axl protein, and Protein S is a ligand of Tyro-3 protein only (Stitt et al., 1995; Varnum et al., 1995). After a while, it is discovered that Gas6 can bind all the members of the TAM family, while Protein S binds on the Tyro-3 and Mer proteins (Godowski et al., 1995; Mark et al., 1996; Nagata et al., 1996; Chen, Carey and Godowski, 1997; Prasad et al., 2006). In several studies investigating Gas6 binding affinity among all three members of the TAM family, it is found that Gas6 bind on the Axl and Tyro-3 with almost the same affinity while it binds to the Mer with 3-10 fold lower affinity (Chen, Carey and Godowski, 1997; Fisher et al., 2005).

The amino acid sequence similarity of the Gas6 and Protein S is around forty-three percent (Stenflo, Lundwall and Dahlbäck, 1987; Dahlbäck and Villoutreix, 2005), and Protein S has thrombin cleavage site as a distinct feature (Stenflo, Lundwall and Dahlbäck, 1987; Dahlbäck and Villoutreix, 2005). The N terminal of the Protein S and Gas6 needs to be carboxylated for the activation. The general structure of the protein has the Gla domain (γ-carboxyglutamic acid), EGF-like repeats, and LG-laminin-G-like domains. When they interact with the host cell receptor, the Gla domain is carbonylated to stabilize the V shape formation of the proteins. Therefore the Gla domain has Ca^{+2} to bind to the receptor on the cell membrane (Mark et al.,

1996; Sasaki et al., 2002a). In the Gas6 protein, some hydrophobic sites are crucial for the effective Axl binding (Sasaki et al., 2002b). There are two LG domains in the Gas6 protein. When Gas6 binds on the Axl, LG1 directly interacts with the receptor. This reaction causes homodimerization of the receptor. It recruits the other Axl, which is bound with the Gas6. This reaction is not directly related to the hydrophobic residues on the Gas6, but they indirectly play an essential role (Sasaki et al., 2006).

2.2 TAM Receptors and Cancer

Cancer disease may be related to many causes like overexpression, abnormal protein function, or many other reasons. TAM receptor genes are the protooncogenes that are why they have a huge role in cancer development and metastasis. The TAM receptors that were taken from the cancer cell lines showed an overexpression pattern by several techniques like Western Blotting, RT-PCR, microarrays, and flow cytometry (Jia et al., 1992). Generally, Tyro-3 protein overexpression resulted in AML (acute myeloid leukaemia) and multiple myeloma. Abnormal Axl expression resulted in the lung, ovarian, liver, breast, colon, prostate, AML, CML, glioblastoma, and renal cell carcinoma. Abnormal expression of Mer resulted in mantle cell lymphoma, melanoma, gastric cancer, and prostate cancer (Liu, Hjelle and Bishop, 1988; Neubauer et al., 1994; Craven et al., 1995; Crosier et al., 1995; Jacob et al., 1999; Rochlitz et al., 1999; Wimmel et al., 2001; Wu, Robinson and Kung, 2004; Shieh et al., 2005; Mahajan et al., 2005; Sainaghi et al., 2005).

Reduction in motility, cell morphology changes, and cell-to-cell communication loss is seen on the Axl expression lacking kinase domain activity in the glioblastoma cells (Vajkoczy et al., 2006). In other studies, EGF/Mer chimeric protein ectopically expressed in murine leukemic cell line showed changes in cell morphology like cell flattening, adherence, and extension of dendrites (Guttridge et al., 2002). Therefore, expression pattern or the expression of the abnormal tissue or cell of TAM receptors showed oncogenic properties in cell morphology. Other than the relation of the kinase activity of TAM receptors and cancer, the extracellular domain of the Axl has a role in the cell-to-cell connection. The extracellular part of the Axl tends to form homophilic interactions.

Interestingly, overexpression of Axl alone did not result in cell aggregation in the mammalian leukaemia cell line (McCloskey et al., 1997). The EGF and/or Gla domain of the Gas6 is bind on the mammalian leukaemia cell line and leaves the LG domain open for the Axl binding. This reaction results in cell aggregation. Therefore, it is seen that cell aggregation is related to the Gas6-Axl interaction together (Figure 2.2.1).

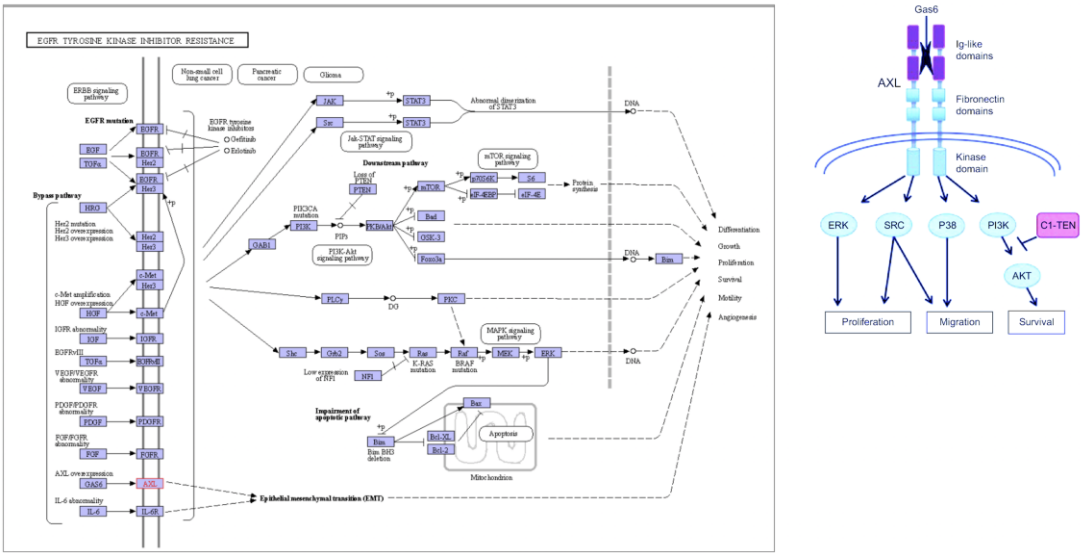

Figure 2.2.1. Gas6/Axl protein complex signalling pathway.

2.3 Computer Aided Drug Design

Drug development is a lengthy process that costs a lot of money and time. The produced compounds are randomly screened in classical drug design approaches. Computers can improve the drug design process with high precision while removing the process's drawbacks. Ninety percent of the drugs which are in the clinical trials are eliminated during the process. Therefore, most of the money spent is waste. Computer power can be utilized to design new compounds or redesign existing ones in drug development. Millions of compounds can be virtually screened, and those that are not effective can be eliminated without investing much money.

2.3.1 Structure-Based Drug Design (SBDD)

Drug design employs a variety of computational methodologies. One of the two main divisions of computer-aided drug design is structure- and ligand-based drug design. Structure-based drug design (SBDD) can be used if the 3D structure of the target protein is already determined using X-ray crystallography or NMR spectroscopy methods. Threading or homology modeling approaches can be used to estimate the structure of the target protein when the structure of the protein is unknown. The amino acid sequence of the protein should be known before using the threading approach. Then, the protein structure is predicted based on the known folding of the linked amino acid sequences. In the homology modeling method, a protein with a known 3D structure is found and utilized as a template for the protein with an unknown structure. The template and target protein sequences are aligned to obtain the 3D protein structure of the target. As a result, a template can be used to anticipate the unknown protein structure.

2.3.2 Molecular Docking Simulations

Molecular docking is a computational approach to predict the preferred binding poses depend on the specific binding cavity on a specific protein. The outcomes of the process are docking poses and docking scores. The docking pose represents the specific pose of a small molecule on the target protein (i.e., macromolecule), and the docking score represents the binding energy of ligand and protein binding. That way, biologically active or inactive molecules are differentiated (Cramer, Christopher J., Horn, 2003).

When calculating the binding energy of the small molecules at the protein, the following equation can be used:

$$\Delta \boldsymbol{G} = \Delta \boldsymbol{H} - \boldsymbol{T}\Delta \boldsymbol{S} \tag{2.1}$$

Here, S term represents the entropy, and H is enthalpy. In this equation, change in entropy is assumed as zero because the ligand has a very small contribution to the system's entropy change (Cramer, Christopher J., Horn, 2003).

$$\Delta \boldsymbol{U} = \Delta \boldsymbol{H} + \boldsymbol{P}\Delta \boldsymbol{V} \tag{2.2}$$

In equation 2.2, V is the volume of the system. The change in the volume is assumed ignorable because the addition of a small molecule almost will not change the system's volume. Thus, the change in binding free energy can be estimated with the change in internal energy when ligand and protein binds to each other.

Molecular docking studies are commonly employed in drug development to investigate the relationship between a small molecule and the target protein. The two outcomes are the result of molecular docking experiments. The interactions between the small molecule and the target protein are one such example. The docking score, which shows the binding free energy of the target protein and the small molecule complex, is the other parameter investigated.

Blind docking refers to docking without the knowledge of the binding site of the ligand. In that case, protein surface can be scanned by the ligands to find optimal binding poses.

There are different available commercial and non-commercial molecular docking programs. Such as the Glide docking program in the Maestro molecular modeling suite offers flexible ligand docking. Flexibility of the ligand during the docking (i.e., conformational change) and binding pocket site can be increased with different ways. Such as in induced fit docking (IFD), partial flexibilities can be gained to the binding pocket residues.

In virtual screening, depending to the size of the screened ligand numbers, different options can be considered. For example, in HTVS (High Throughput Virtual Screening) millions of molecules can be screened at a specific protein site with reasonable time. With advanced scoring functions (i.e., Glide/SP (standard precision), or XP (extra precision)) more precise results can be searched for small number of compounds.

2.3.3 Ligand-Based Drug Design (LBDD)

By analyzing the interactions of the ligands with the active site residues of the protein, ligand-based drug design (LBDD) is indirectly used to develop pharmacologically active molecules. In the LBDD, 3D QSAR and pharmacophore modeling are commonly used approaches.

The goal of the ligand optimization procedure is to improve the interaction between the target protein and the lead compounds. Scientists can use CADD to optimize lead compounds not only in ligand-based drug design but also in structure-based drug design.

2.3.4 Molecular Dynamics (MD) Simulations

MD simulations are powerful computational technique for predicting how a molecule's velocity and position vary over time. In MD simulations, interactions between molecules are specified using a collection of Newtonian classical mechanics-based models. These "classical molecular models" treat molecules as mass-and-electric-charged particles that interact with other "particles." The system is then replicated, and the particle's trajectory is recorded. Deterministic approaches are employed in MD simulations to solve classical mechanics equations of motion to construct a dynamical and ongoing trajectory of a biomolecular system. A trajectory file can be generated at the end of an MD simulation that interprets all the dynamic variables and their changes over time.

2.4 In Silico Research of AXL

Sarukhanyan et al. investigated the inhibition of the Axl receptor to prevent dimerization and virus entry in their study. Axl is also involved in the virus's entry into the host cell. They synthesized new molecules (RU-301, RU-302 (Kimani et al., 2017)) and compared their activity with the experimentally confirmed substances such as Warfarin (Son et al., 2014) and R428 (Holland et al., 2010). The molecules they designed is the derivative of the R428. They used molecular docking and molecular

dynamics (MD) simulations, and MM/GBSA (Molecular Mechanics Generalized Born Surface Area), and MM/PBSA (Molecular Mechanics Poisson-Boltzmann Surface Area) computations in their research (Sarukhanyan, Shityakov and Dandekar, 2018).

In another study of the same team, they investigated the effect of Axl on cancer disease. (Sarukhanyan, Shityakov and Dandekar, 2020) R5 (a derivative of R428), is a newly developed molecule, has been identified as the most promising inhibitor against the Axl target. Three molecular docking techniques were used, and MD simulations and MM/PBSA and MM/GBSA calculations were performed using an implicit solvation system. The R5 compound was also found to have an affinity for the ABL1 and Tyro3 protein targets. All the findings indicate that the R5 compound could be a viable target in treating malignant cancers. As a result, they discussed crucial interactions for figuring out novel inhibitors and the Axl-Gas6 signalling complex's molecular structure. It is necessary to do further research and investigation to develop new inhibitors for Axl-Gas6 protein signalling (Sarukhanyan, Shityakov and Dandekar, 2020).

Chapter 3

Methodology

3.1 Protein Preparation

The protein complex of the AXL-GAS6 protein complex crystal was downloaded from the PDB (Protein Database, PDB: 2C5D). The Ala676 and Leu217 residues were deleted. The missing side chains and loops were filled with the Prime module of the Maestro. The pH was arranged as in the physiological condition (pH: 7.4). The disulphide bonds were regenerated. Missing hydrogens were added, and the terminal residues were capped. Water molecules beyond 5.0 Å from hetero groups were deleted. The bond orders were assigned. Zero-order bonds to metals were created. The hydrogen bonds were assigned as pH 7.4 using PROPKA. (Olsson et al., 2011) Then, the protein is relaxed with nonhydrogen atoms in the protein with the threshold convergence of 0.30 Å. The B and D chains were deleted.

3.2 Ligand Preparation

Before the ligand docking, the FDA drugs, and compounds in clinical investigation and Peptidomimetic databases from ChemDiv were virtually screened for their toxicity and anti-cancer therapeutic activities with the Clarivate Analytics' MetaCore/MetaDrug platform (https://portal.genego.com/). This tool is intended to create a detailed profile of a compound's pharmacokinetic and pharmacodynamic features. There are 25 common diseases binary QSAR models and 26 toxicities binary QSAR models that may determine a compound's Tanimato Prioritization (TP) value based on how similar it is to the QSAR models' training and test sets. The MetaCore™ /MetaDrug™ platform's main goal is to predict the major metabolites of an input structure and how their binding affects the human body's essential enzymes. It's a platform that leverages QSAR to anticipate small-molecule pharmacokinetic and pharmacodynamic characteristics. The threshold for anti-cancer therapeutic activity was chosen as 0.50. In MetaCore/MetaDrug, therapeutic activity predictions are

computed with the binary QSAR models. Cancer-QSAR models has following statistical results: Training set N=886; Test set N=167; Sensitivity= 0.89; Specificity=0.83; Accuracy=0.86; MCC=0.72. After all the toxicity (in 26 different available toxicity QSAR models at the MetaCore) and therapeutic activity eliminations, 1341 peptidomimetics out of 36711 and 1089 FDA molecules library out of 6733 left. Selected molecules were prepared with the LigPrep module of the Maestro. The OPLS 2005 force field was used, and possible protonation states were generated at a target physiological pH of 7.4. The molecules were desalted, and tautomers were generated.

3.3 Novel Peptide Development Study

The key residues essential for GAS6-AXL major binding were determined. They are R308, R310 and K312. They are selected on the chain of Gas6 protein. The three residues kept constant, and the nearby residues on the same chain added to create the new peptide sequences. The stable part on the Gas6 is RLRFK. The sequence on the Gas6 that is considered to trim is TPVIRLRFKRLQ. Also, the sequence has a β-sheet structure. The peptides intended to create in 7, 8, 9 and 10 residues in length. Therefore, trimmed sequences are TPVIRLRFKR, TPVIRLRFK, PVIRLRFKR, RLRFKRLQ, VIRLRFKR, PVIRLRFK, IRLRFKR, VIRLRFKRL, IRLRFKRL and VIRLRFK. The N terminus and C terminus of the peptides were designed as the $NH3^{+}$ and $CONH_2$, respectively. Then, they were prepared with the LigPrep module of the Maestro. The pH is arranged as physiological conditions. OPLS2005 force field was used. Then, they were energetically minimized using the MacroModel module of the Maestro.

3.4 GLIDE/SP Docking

Before the SP docking, receptor grid was generated using the Maestro Glide module. Six systems were prepared as A, C only, and AC chains together in two different binding sites. (i.e., major, and hydrophobic interface binding sites). The grid generated around the Arg308, Arg310, Lys312 in Gas6; Glu56 and Glu59 in Axl for

the major binding site. For the hydrophobic interface, the grid is formed around Thr46, Thr77, Val92, Gln94, and Arg96 in Axl; 446-459, Ile307, Leu309, Phe311, Thr461, and Met468 in Gas6. Before the peptide docking, a protein grid was generated suitable for the peptide docking.

In the Glide module, SP Docking was used. The initial charges of the prepared protein were used. Only ligands were used as flexible.

3.5 Molecular Dynamics (MD) Simulation

In molecular dynamics (MD) simulations, the system was built using the SPC (simple point charge) solvent model using the Desmond. (Bowers et al., 2006) The simulation box was used as orthorhombic (10 Å from edges of protein was used to construct the simulation boxes). The OPLS2005 force field was used. 0.15 M NaCl salt solution was used and extra Na^+ ions were added to neutralize the system. 2 fs was used as time step. Fifty ns simulation time was chosen for the short simulations. Fifty ns time intervals were arranged, and total of 1000 frames were saved throughout the simulations. The temperature during the simulation was kept as 310 K, and the pressure was arranged as 1.01325 bar. The same procedure was applied for the long simulations with 100 ns total production simulation times. Correspondingly, for peptides, 50 ns was used for short simulations and 200 ns was used for long MD simulations.

3.6 MM/GBSA Calculations

After MD simulations, 100 frames out of 1000 saved trajectory frames were taken from the simulations. The Prime module of the Maestro was used for MM/GBSA calculations. The polar hydrogens with 3.0 Å were flexed, and initial ligand charges were used. Average MM/GBSA values were calculated.

Chapter 4

Findings

4.1 Screening of the Peptidomimetics and FDA Molecule Libraries

After the filtration of databases using binary QSAR models, 1341 peptidomimetic compounds from ChemDiv and 1089 FDA drugs and compounds in clinical investigations from NIH's library were used in docking simulations. Table 4.1.1 shows results of top-docking scored compounds at chain A. In the table, average MM/GBSA scores of corresponding compounds for short (50 ns) and for long (100 ns) simulations were also tabulated. Two different binding sites (sites 1 and 2, hydrophobic interface, and major binding sites, respectively) were considered at the docking (Figure 4.1.1).

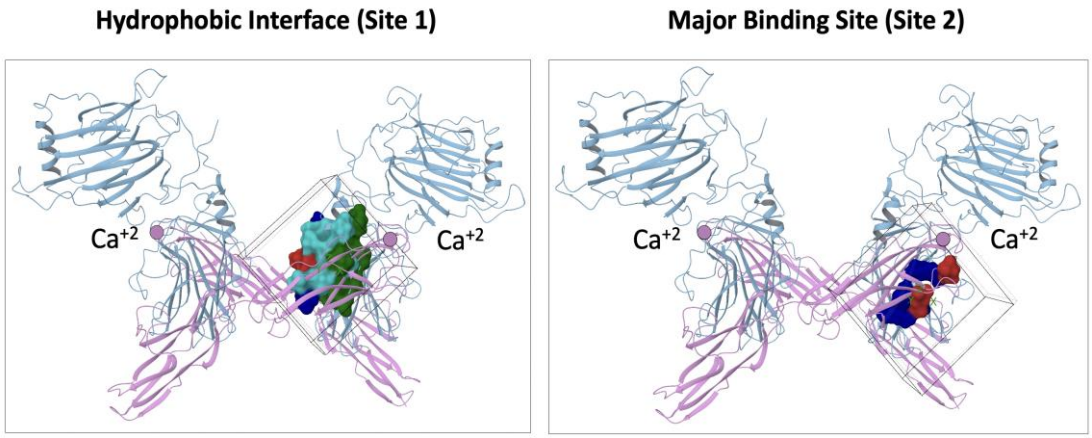

Figure 4.1.1. Two binding sites (sites 1 and 2) at the Gas6/Axl complex (Gas6 is represented with blue, and Axl is represented with pink colour.

On the Table 4.1.1, on site 1, G842-0689, represented the highest negative MM/GBSA score (-88,89 kcal/mol) after 100 ns MD simulations. Positive control compounds (i.e., reference compounds) were used to compare the docking scores and average MM/GBSA scores. Reference molecules were RU-301 and RU-302.

In addition, it is found that compound F723-0087 has more negative MM/GBSA score (-86,78 kcal/mol) than the RU-301 (-74,17 kcal/mol). L998-0110, G566-1097, L998-0042, Saralasin, Gonadorelin, Argiprestocin, Linezolid, and Saquinavir has more negative GBSA scores than the other reference molecule (RU-302).

On site 2, Nafarelin, has the most negative MM/GBSA score with -97,32 kcal/mol. Sincalide, Goserelin, and Oxytocin have higher negative MM/GBSA scores than -90,00 kcal/mol.

Table 4.1.2 shows corresponding results at the C chain. Compounds F044-0077, D675-0102, L748-0628, G288-0106, and Pentagastrin have more negative MM/GBSA scores than RU-301 and RU-302 molecules on the site 1. On site 2, Abarelix, Argipressin, and Desmopressin have more negative scores than -70,00 kcal/mol.

In Table 4.1.3, the AC chain together is used. On site 1, Saquinavir and Gonadorelin have a higher negative score than RU-301 (-78,04 kcal/mol). On the site 2, Histrelin, Leuprorelin, Argiprestocin, Polymyxin B1, and Argipressin has higher negative average MM/GBSA scores than -70,00 kcal/mol. The most negative MM/GBSA score on site 2 was found for the Histrelin, with the highest binding score among all the systems with a -108,42 kcal/mol.

Table 4.1.1

The system A Chain only (Gas6 protein).

Site 1 (hydrophobic)				Site 2 (major)			
2D	Name	Glide SP-Docking (kcal/mol)	MM/GBSA Scores (100 ns) (kcal/mol)	2D	Name	Glide SP-Docking (kcal/mol)	MM/GBSA Scores (100 ns) (kcal/mol)
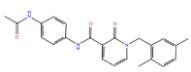	G842-0689	-7,13	-88,89	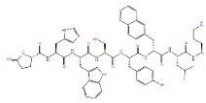	Nafarelin	-8,88	-97,32
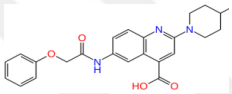	F723-0087	-7,09	-86,78	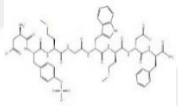	Sincalide	-8,13	-97,28
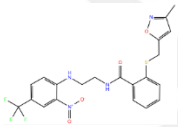	RU-301	-4,78	-74,17	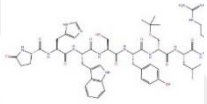	Goserelin	-10,07	-93,04
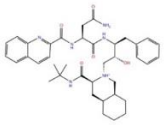	Saquinavir	-7,78	-72,41	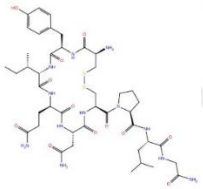	Oxytocin	-8,80	-90,97
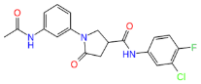	L998-0110	-7,04	-70,66	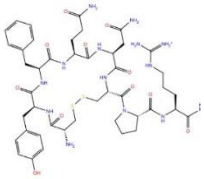	Argipressin	-7,87	-76,10
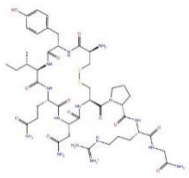	Argipresticin	-7,45	-69,95	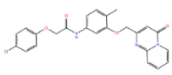	G756-0361	-5,76	-68,94
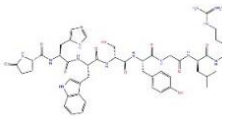	Gonadorelin	-8,13	-66,21	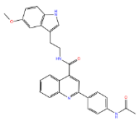	L036-0366	-5,74	-66,66
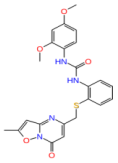	G566-1097	-6,97	-64,79	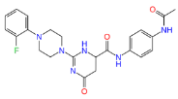	F019-5539	-5,83	-62,45

Site 1 (hydrophobic)				Site 2 (major)			
2D	Name	Glide SP-Docking (kcal/mol)	MM/GBSA Scores (100 ns) (kcal/mol)	2D	Name	Glide SP-Docking (kcal/mol)	MM/GBSA Scores (100 ns) (kcal/mol)
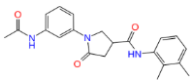	L998-0042	-7,78	-62,37	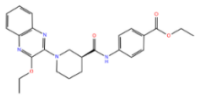	D537-0300	-5,72	-58,31
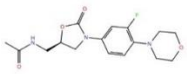	Linezolid	-8,16	-61,27	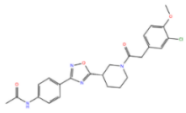	L912-0124	-5,91	-46,31
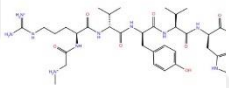	Saralasin	-8,44	-38,61				
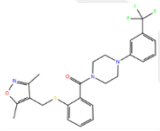	RU-302	-3,06	-35,97				

Table 4.1.2

The system C Chain only (Axl protein).

Site 2(major)				Site 2(major)			
2D	Name	Glide SP-Docking (kcal/mol)	MM/GBSA Scores (100 ns) (kcal/mol)	2D	Name	Glide SP-Docking (kcal/mol)	MM/GBSA Scores (100 ns) (kcal/mol)
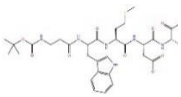	Pentagastrin	-5,69	-66,12	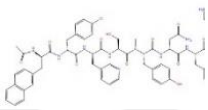	Abarelix	-7,42	-92,12
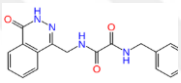	F044-0077	-4,68	-43,77	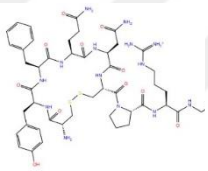	Argipressin	-7,33	-73,03
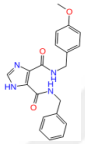	D675-0102	-4,49	-42,69	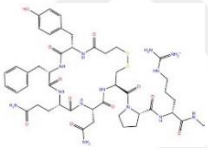	Desmopressin	-7,69	-70,93
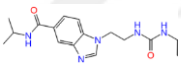	L748-0628	-4,94	-41,74	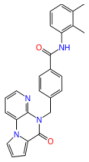	E524-1587	-5,42	-67,16
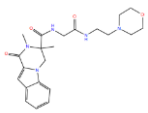	G288-0106	-4,85	-40,09	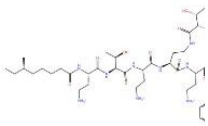	Polymyxin B1	-7,44	-66,42
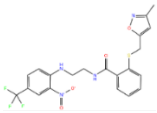	RU-301	-2,84	-35,68	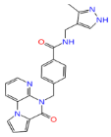	E524-1716	-5,33	-64,04
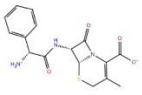	Cefalexin	-4,68	-33,82	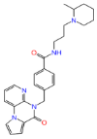	E524-1731	-5,70	-62,32
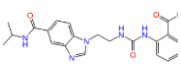	L748-0604	-4,48	-33,52	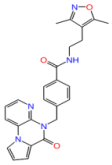	E524-1708	-5,34	-55,87

Site 2(major)				Site 2(major)			
2D	Name	Glide SP-Docking (kcal/mol)	MM/GBSA Scores (100 ns) (kcal/mol)	2D	Name	Glide SP-Docking (kcal/mol)	MM/GBSA Scores (100 ns) (kcal/mol)
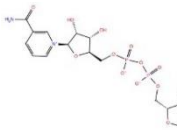	Dinucleotide dihydronicotinamide adenine	-4.75	-32,19	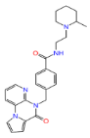	E524-1737	-5,45	-51,32
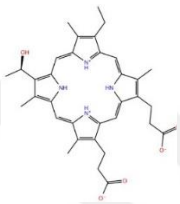	Photofrin	-4,75	-31,27	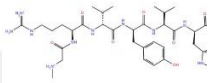	Saralasin	-7,06	-43,72
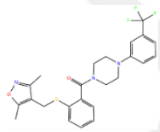	RU-302	-2,20	-30,04				
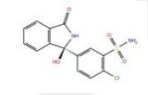	Clodronic acid	-5,27	-27,44				

Table 4.1.3

The system AC Chain together (Axl-Gas6 protein).

Site 1 (hydrophobic)				Site 2 (major)			
2D	Name	Glide SP-Docking (kcal/mol)	MM/GBSA Scores (100 ns) (kcal/mol)	2D	Name	Glide SP-Docking (kcal/mol)	MM/GBSA Scores (100 ns) (kcal/mol)
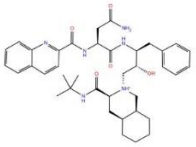	Saquinavir	-8,55	-90,62	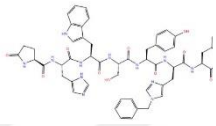	Histrelin	-11,69	-108,42
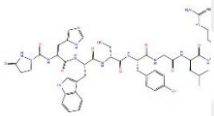	Gonadorelin	-8,10	-81,56	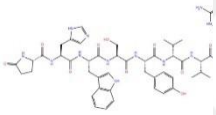	Leuprorelin	-10,13	-85,94
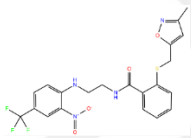	RU-301	-6,50	-78,04	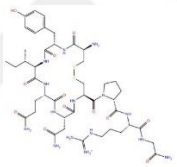	Argipressocin	-7,81	-84,27
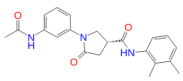	L998-0042	-8,35	-74,44	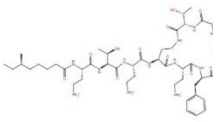	Polymyxin B1	-9,45	-82,47
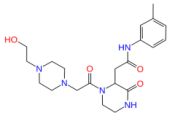	D718-0741	-7,61	-70,94	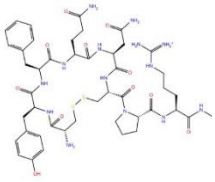	Argipressin	-8,02	-75,17
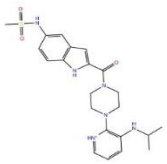	Delavirdine	-7,97	-70,00	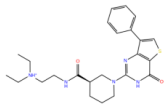	L381-0578	-6,38	-67,23
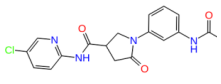	L998-0012	-7,96	-68,99	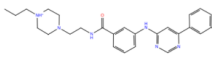	F725-0072	-5,55	-62,43
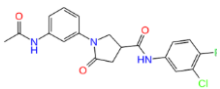	L998-0110	-7,72	-65,57	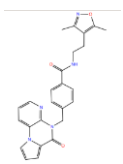	E524-1708	-5,64	-60,96

Site 1 (hydrophobic)				Site 2 (major)			
2D	Name	Glide SP-Docking (kcal/mol)	MM/GBSA Scores (100 ns) (kcal/mol)	2D	Name	Glide SP-Docking (kcal/mol)	MM/GBSA Scores (100 ns) (kcal/mol)
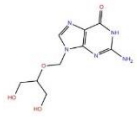	Ganciclovir	-8,78	-61,77	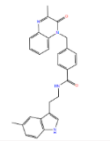	F671-0144	-5,55	-58,63
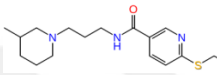	L161-0175	-7,74	-59,60	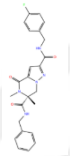	E852-1289	-5,87	-53,79
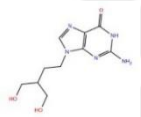	Penciclovir	-8,781	-54,13				
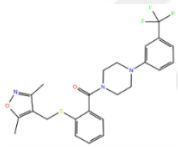	RU-302	-2,49	-29,69				

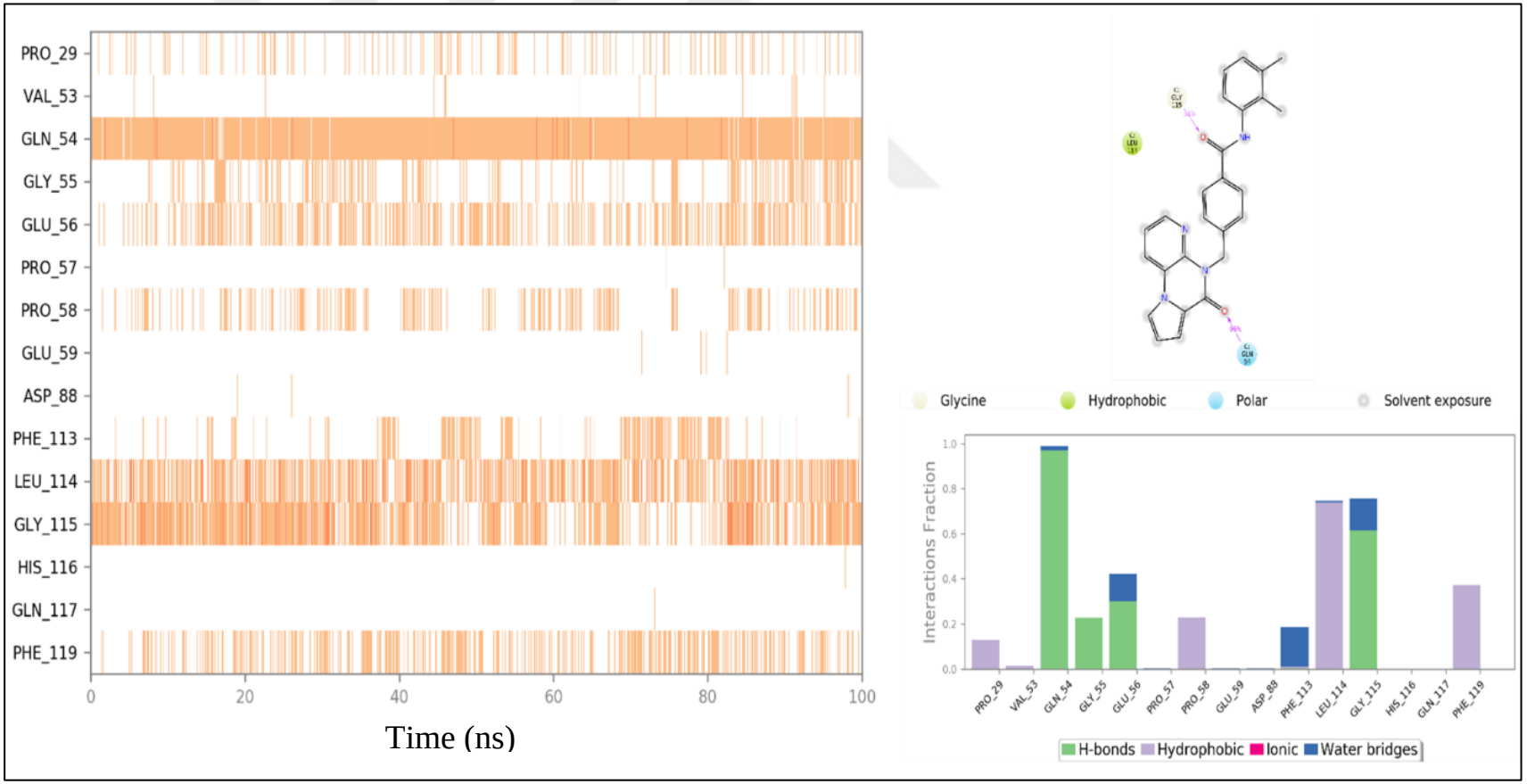

Figure 4.1.2. The interaction diagram of the E524-1587 on the site 2 of the C chain during the 100 ns MD simulations.

In Figure 4.1.2, the hit compound E524-1587 molecule on site 2 of the C chain is depicted. After the 100 ns MD simulations, the representative frame was chosen with nearest RMSD to the average frame during the simulations. The interaction strength throughout the simulations is represented with the plot. The intensity of the color shows how strong the interaction is. Here, Gln54, Leu114, and Gly115 residues showed strong binding contacts with the ligand throughout the 100 ns simulations. Also, there is a bar graph that shows which interaction formed with which residue at the binding pocket (Figure 4.1.2, right-bottom). This molecule formed H-bonds, hydrophobic interactions, and water bridges with the binding pocket residues. While ligand forms hydrogen bonds with Gln54, Glu56, and Gly115 (from backbone), it constructs hydrophobic interactions mainly with Leu114 and Phe119. On top of the bar graph, there is a 2D representation of the molecule and interaction percentages of the residues. Gln54 interacted ninety-six percent of the 100 ns MD simulation time with the molecule, whereas Gly115 interacted with the molecule sixty-one percent of the time.

In Figure 4.1.3, the representative frame of the 100 ns MD simulations of the E524-1587 molecule and site 2 of the C chain is represented. The 3D structure of the protein with surface representation and molecule inside the binding cavity of major binding site can be seen. On the representative frame, Gln54, Gly115, and Glu56 formed hydrogen bonds with the molecule.

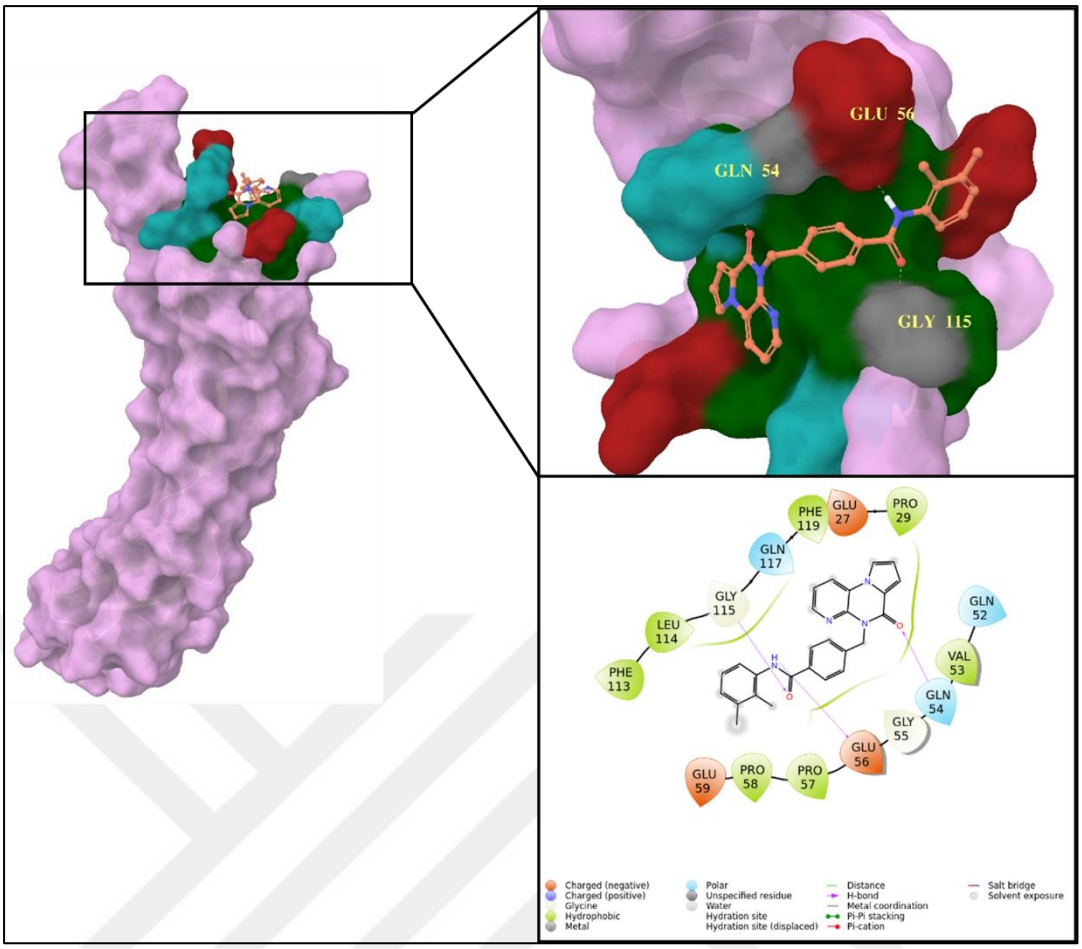

Figure 4.1.3. The representative frame of the 100 ns MD simulation of the E524-1587 on the site 2 of the Axl protein.

In the Figure 4.1.4, L998-0042 on site 1 of the AC chain is depicted. After the 100 ns MD simulations, the representative frame was chosen to depend on the proximity to the average frame. Here, Trp448, Ile458, and Gln459 showed strong binding interactions during the 100 ns simulations. Also, bar graph shows which residues interacted with what type of bond formed. This molecule formed H-bonds, hydrophobic interactions, and water bridges. Gln459 formed mainly hydrogen bonds and water bridges. On top of the bar graph, there is a 2D representation of the molecule and interaction percentages of the residues. Gln459 interacted eighty-two percent of the 100 ns MD simulation time with the molecule, whereas Ile458 interacted with the molecule eighty-five percent of the time.

In Figure 4.1.5, the representative frame of the 100 ns MD simulations of the L998-0042 hit molecule and site 1 of the AC chain are represented. The 3D structure of the protein with surface representation and molecule at the binding site can be seen. On the representative frame, Gln459 and Ile458 formed hydrogen bonds with the molecule.

In Figure 4.1.6, Abarelix compound on site 2 of the C chain is depicted. Throughout the simulations, Glu59 and Phe113 residues showed strong binding interactions. Compound formed hydrogen bonds, ionic interactions, hydrophobic interactions, and water bridges. Glu59 constructed hydrogen bonds, ionic interactions, and water bridges with the ligand. Glu59 interacted fifty-two percent of the 100 ns MD simulation time with the hit molecule, whereas Phe113 interacted with the molecule fifty percent during the simulations.

In Figure 4.1.7, representative frames of the 100 ns MD simulation of the Abarelix molecule and site 2 of the C chain are depicted. The 3D structure of the target protein with surface representation and the ligand at the binding site can be seen. Glu59, His61, Trp62, Gly115, and Phe113 formed hydrogen bonds with the molecule on the representative frame.

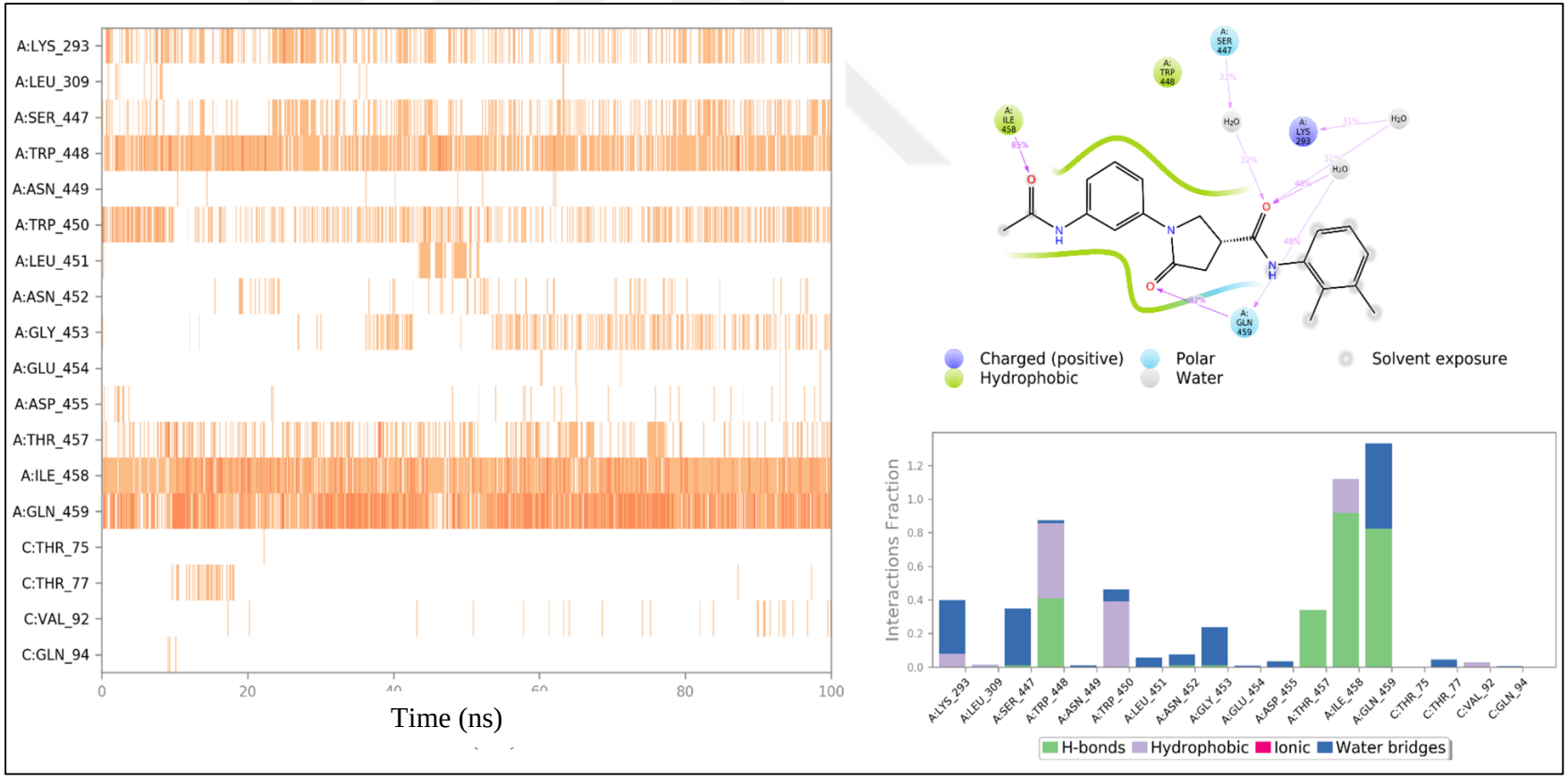

Figure 4.1.4. The interaction diagram of the L998-0042 on the site 1 of the Axl-Gas6 protein during the 100 ns MD simulations.

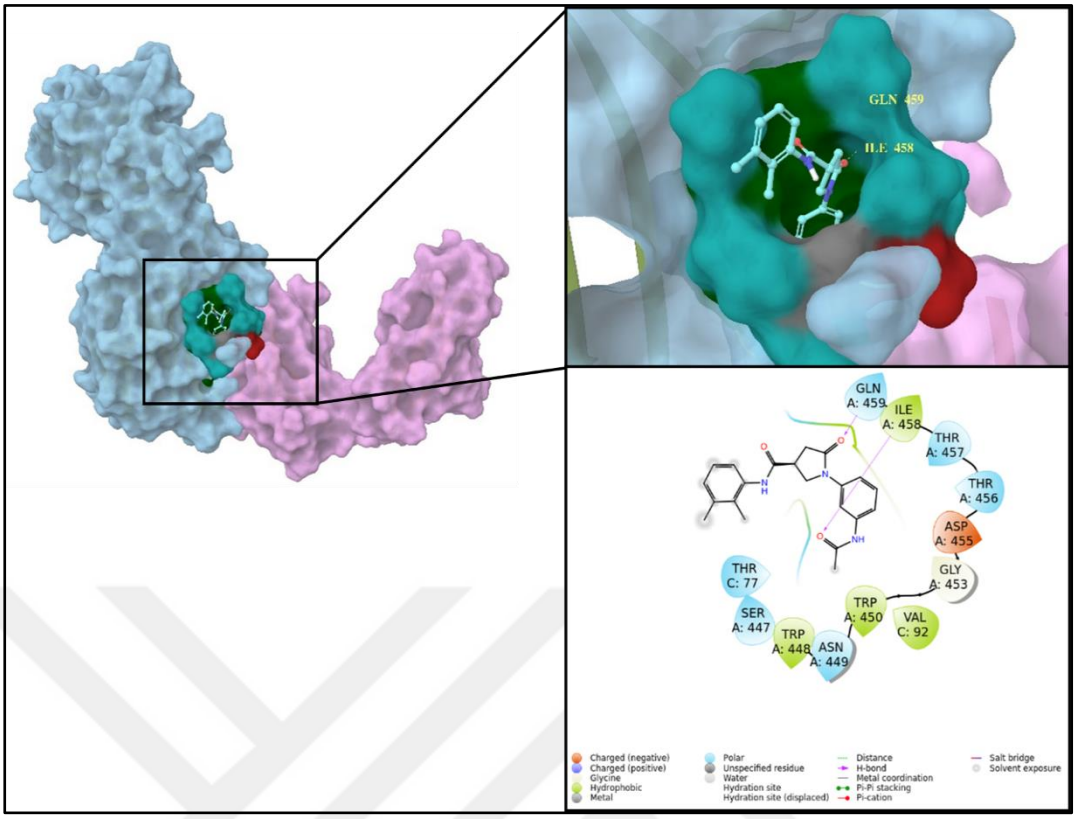

Figure 4.1.5. The representative frame of the 100 ns MD simulation of the L998-0042 on the site 1 of the Axl-Gas6 protein.

In Figure 4.1.8, Saquinavir on site 1 of the AC chain is represented. Trp448 and Gln459 residues at the binding pocket showed strong binding interactions throughout the 100 ns simulations. Trp448 formed hydrogen bonds, hydrophobic interactions, and water bridges with the ligand. Trp448 interacted fifty-seven percent with the ligand throughout the MD simulation time, whereas Gln459 interacted with the molecule sixty-one percent of the time.

In Figure 4.1.9, representative frames of the 100 ns MD simulation of the Saquinavir molecule and site 1 of the AC chain are depicted. The 3D structure of the target protein with surface representation and the ligand at the binding site can be seen. Ser447 and Gln459 formed hydrogen bonds with the molecule on the representative frame.

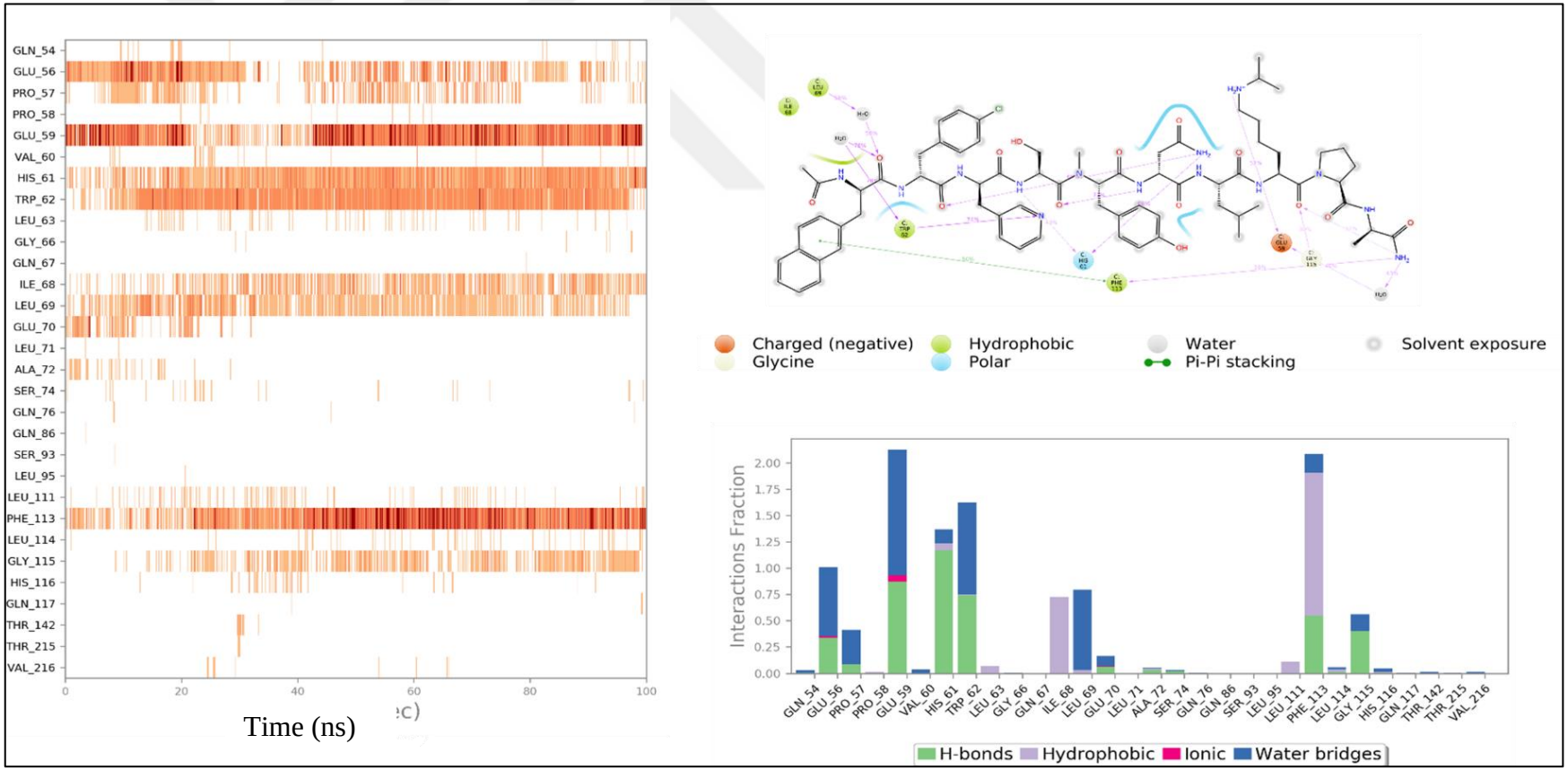

Figure 4.1.6. The interaction diagram of the Abarelix on the site 2 of the C chain during the 100 ns MD simulations.

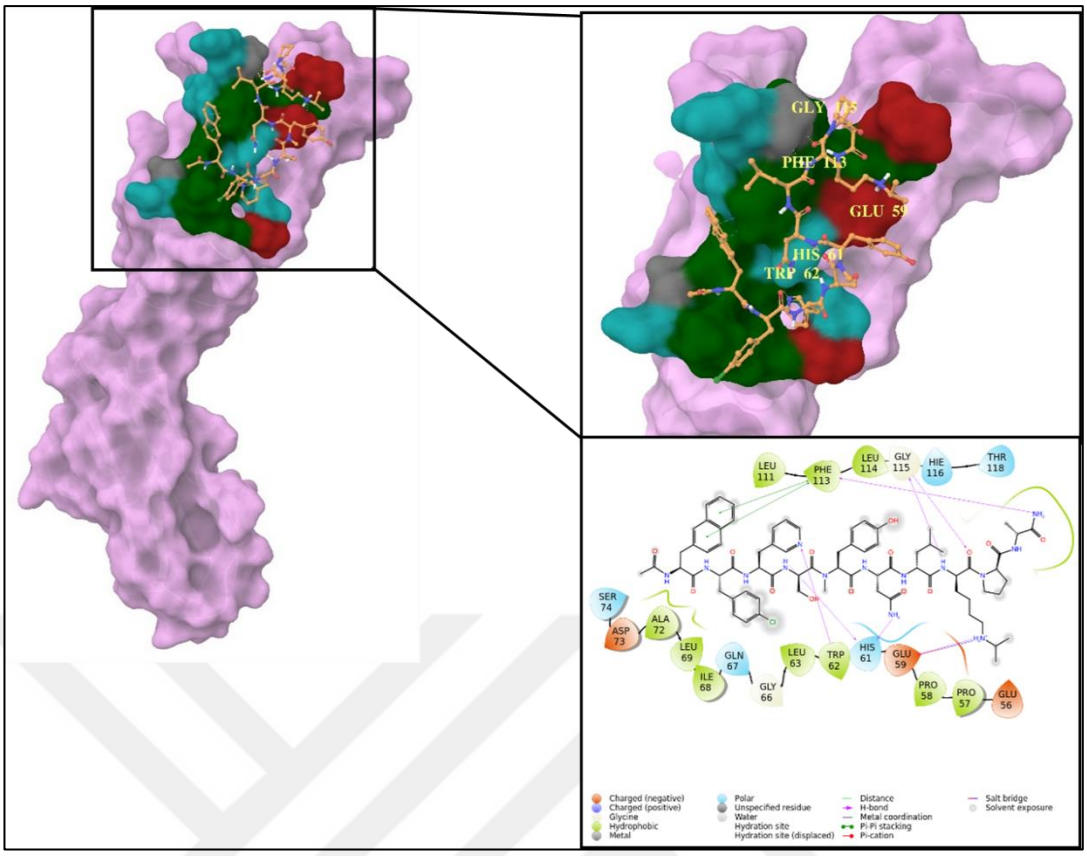

Figure 4.1.7. The representative frame of the 100 ns MD simulations of the Abarelix on the site 2 of the Axl protein.

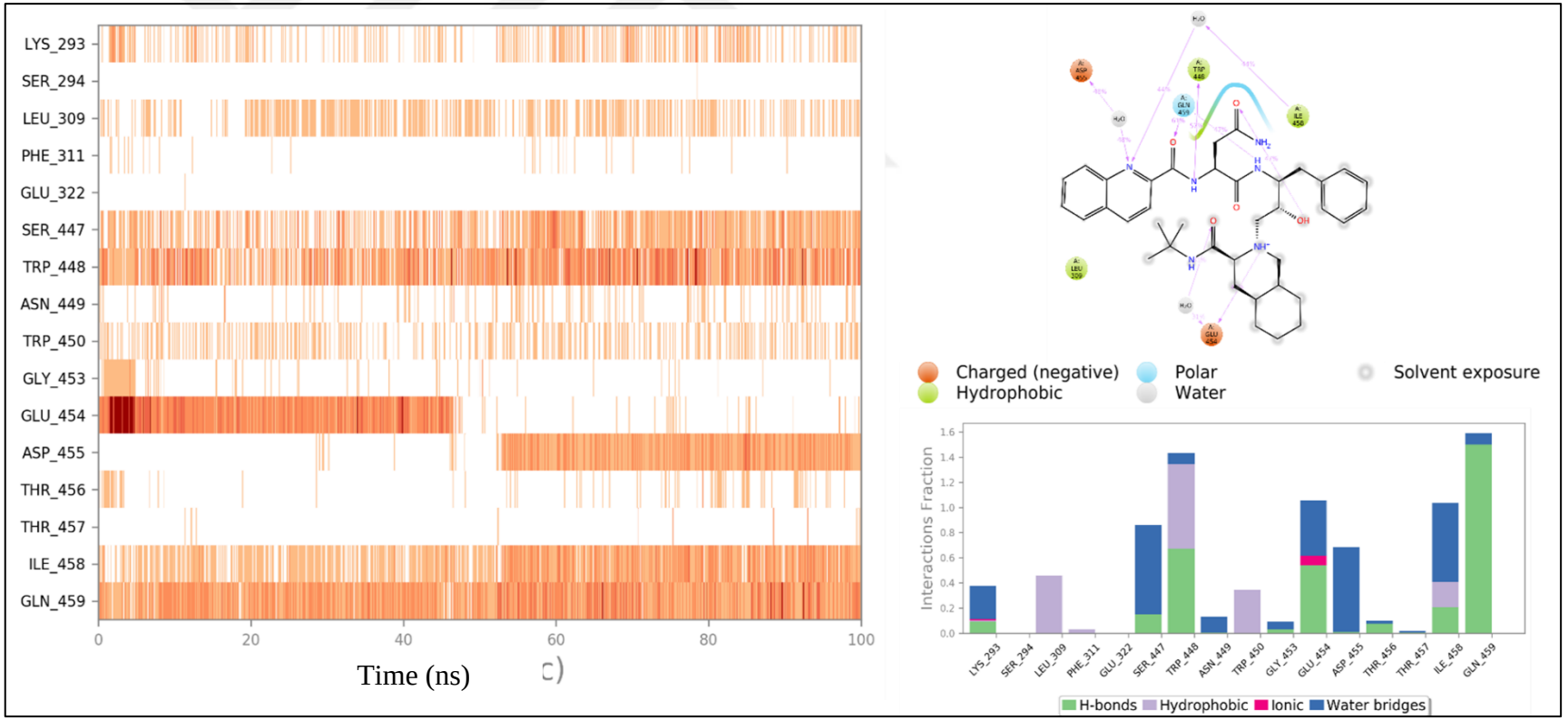

Figure 4.1.8. The interaction diagram of the Saquinavir on the site 1 of the AC chain during the 100 ns MD simulations.

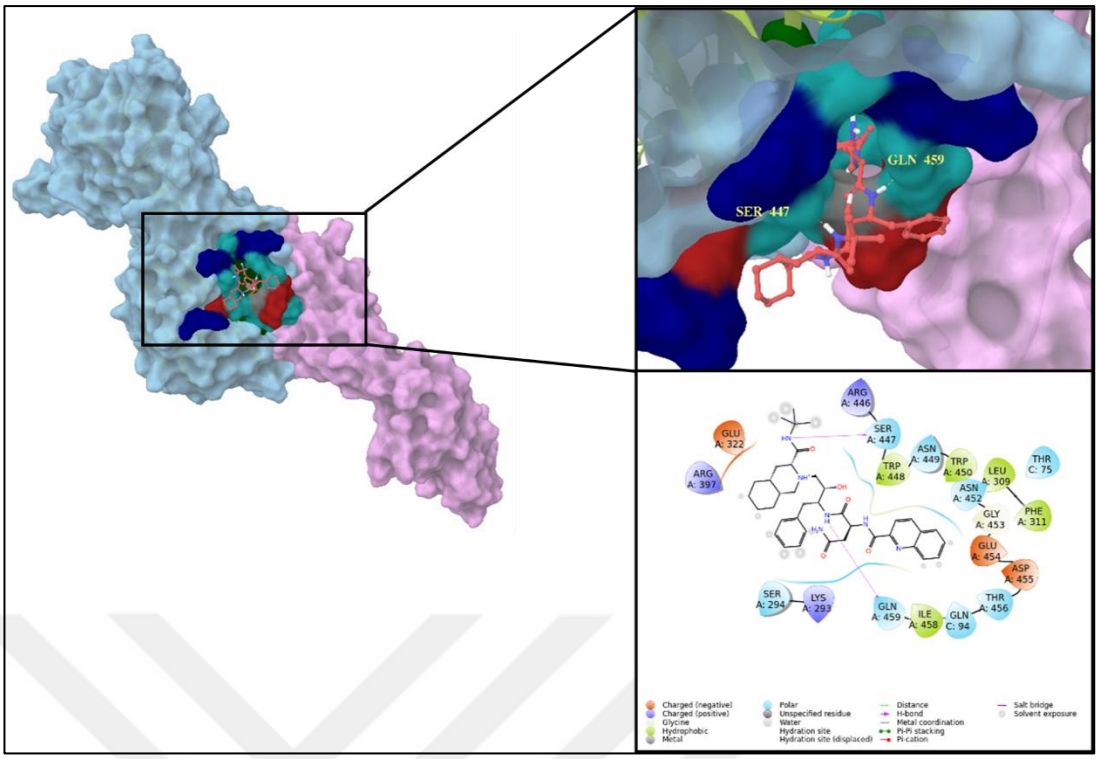

Figure 4.1.9. The representative frame of the 100 ns MD simulations of the Saquinavir on the site 1 of the Axl-Gas6 protein.

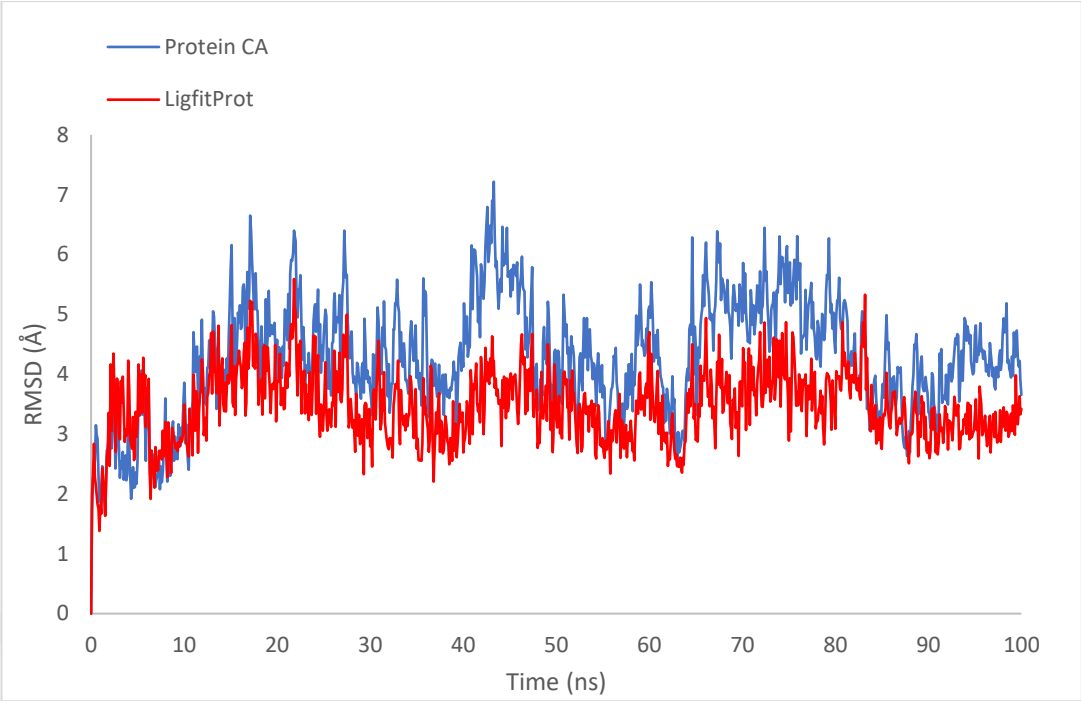

Figure 4.1.10. The RMSD graph of the Saquinavir on the site 1 of the AC chain of the Axl-Gas6 protein.

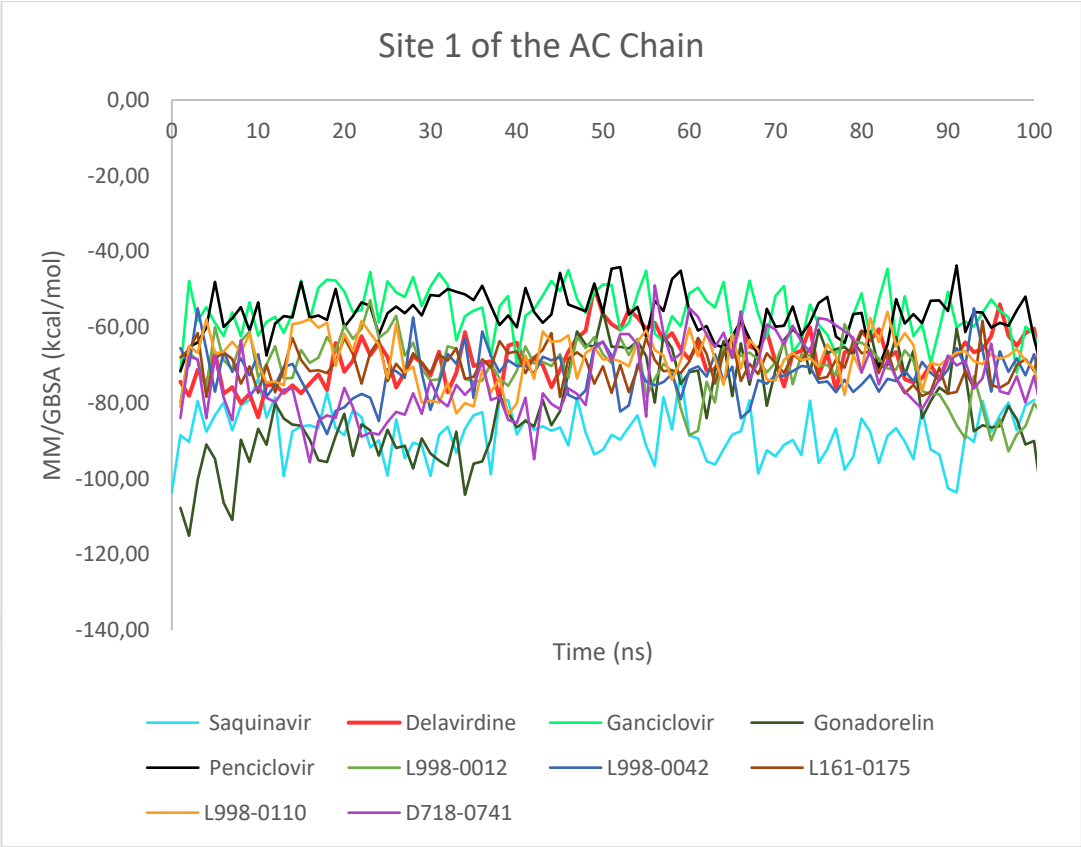

Figure 4.1.11. MM/GBSA-time graph of the Saquinavir, Gonadorelin, Delavirdine, Ganciclovir, Penciclovir, L998-0012, L998-0042, L161-0175, L998-0110 and D718-0741 on the site 1 of the AC Chain.

On the Figure 4.1.11 MMGBSA-time graph of the Saquinavir, Gonadorelin, Delavirdine, Ganciclovir, Penciclovir, L998-0012, L998-0042, L161-0175, L998-0110 and D718-0741 on the site 1 of the AC Chain is seen. Penciclovir and Ganciclovir has the lowest negative MM/GBSA scores while Saquinavir has the highest negative score on the site 1 of the AC chain. Scores are between -60 and -100 kcal/mol.

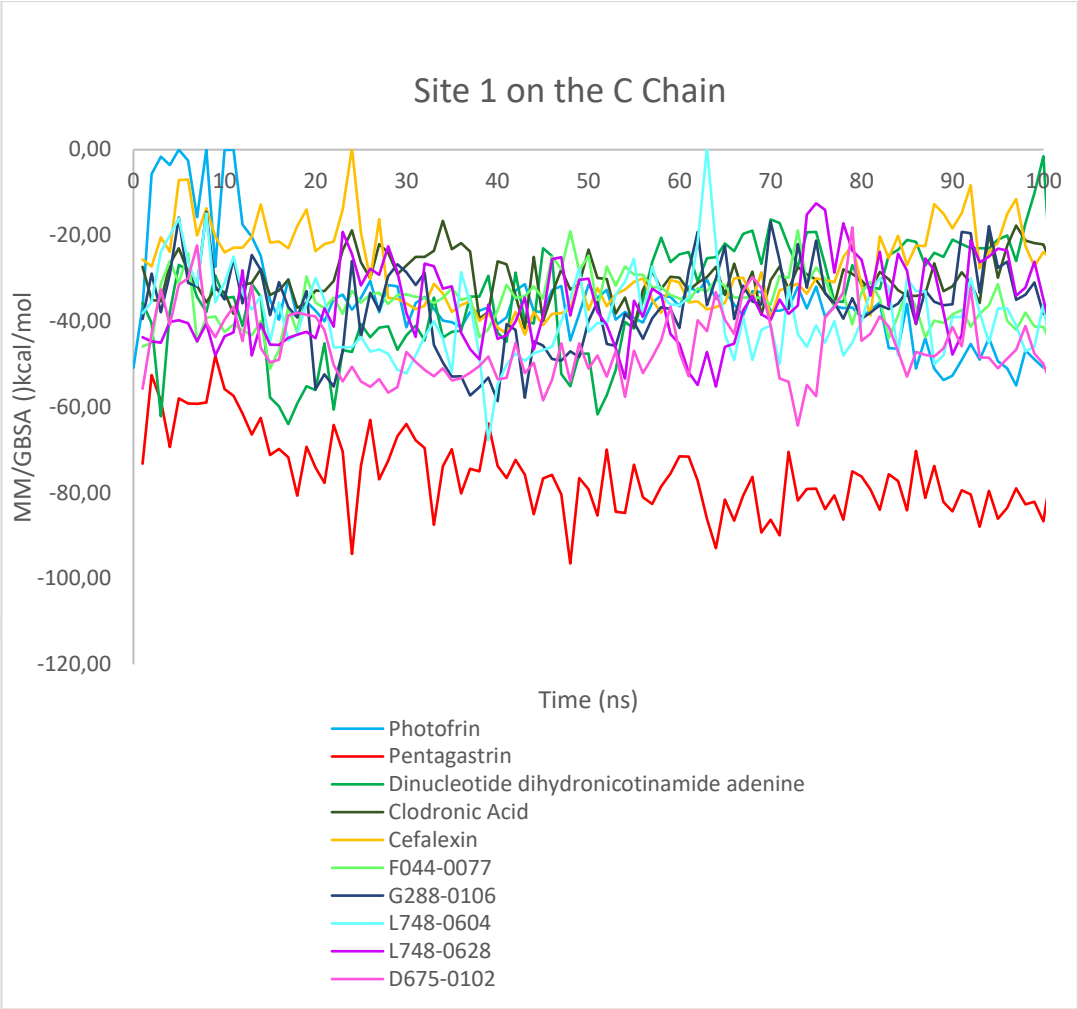

Figure 4.1.12. MM/GBSA-time graph of the Photofrin, Pentagastrin, dinucleotide dihydronicotinamide adenine, Cefalexin, G288-0106, L748-0628, F044-0077, L748-0604 and D675-0102on the site 1 of the C Chain.

On the Figure 4.1.12, MM/GBSA-time graph of the Photofrin, Pentagastrin, dinucleotide dihydronicotinamide adenine, Cefalexin, G288-0106, L748-0628, F044-0077, L748-0604 and D675-0102on the site 1 of the C Chain is seen. Pentagastrin has the highest negative score. Generally, molecules accumulated between -20 and -50 kcal/mol which is not strong binding score. Other than Pentagastrin, molecules do not seem to establish strong interactions on the site 1 of the C chain.

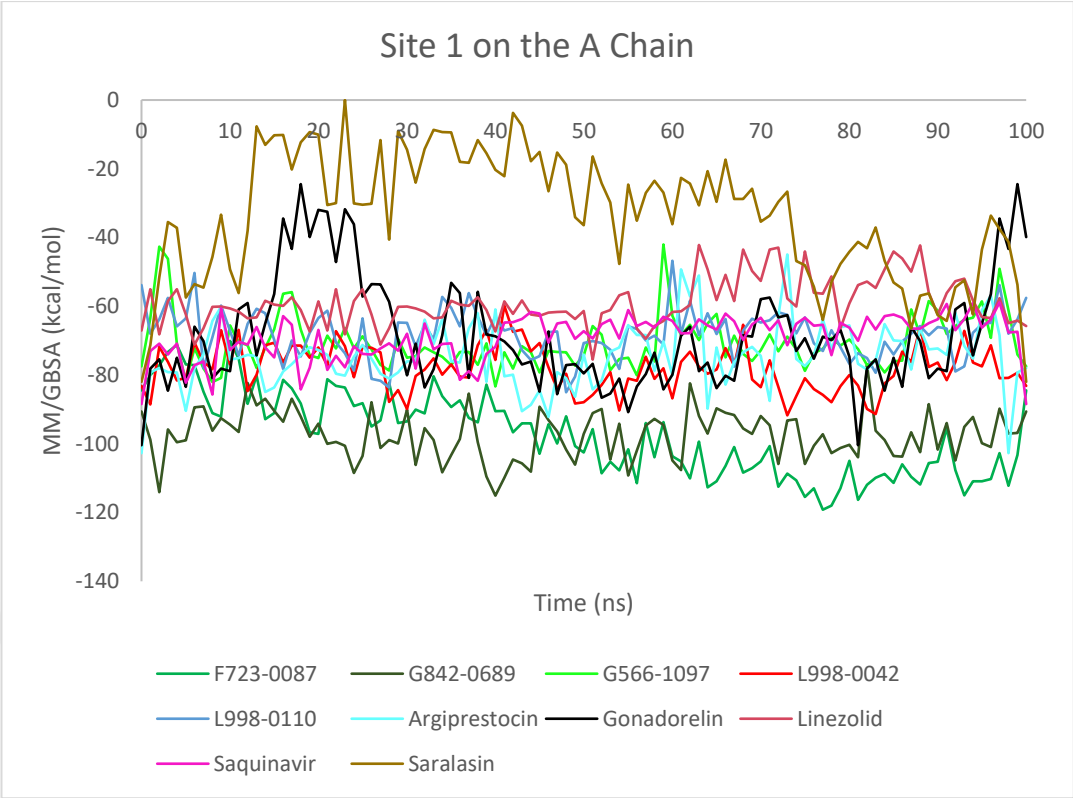

Figure 4.1.13. MM/GBSA-time graph of the F723-0087, G842-0689, G566-1097, L998-0042, L998-0110, Argiprestocin, Gonadorelin, Linezolid, Saquinavir and Saralasin on the site 1 of the A Chain.

On the Figure 4.1.13, MM/GBSA-time graph of the F723-0087, G842-0689, G566-1097, L998-0042, L998-0110, Argiprestocin, Gonadorelin, Linezolid, Saquinavir and Saralasin on the site 1 of the A Chain is seen. Saralasin molecule has the lowest MM/GBSA score throughout the simulation. G842-0689 and F723-0087 has the highest negative MM/GBSA scores shown as the yellow and green, respectively.

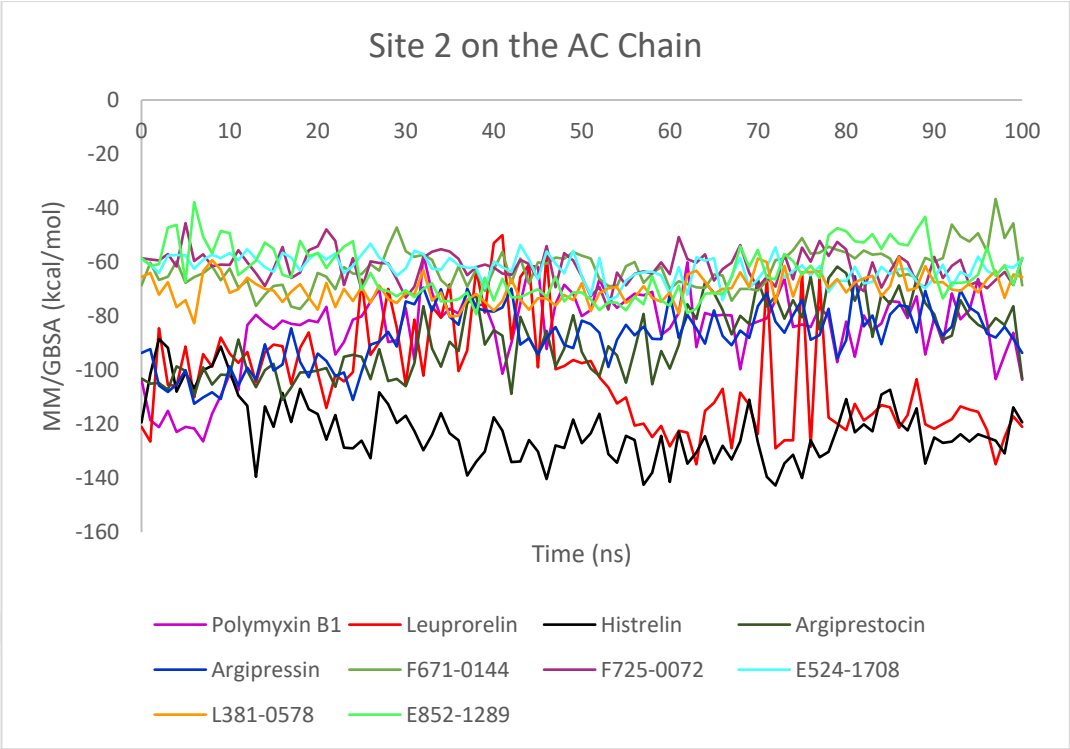

Figure 4.1.14. MM/GBSA-time graph of the Polymyxin B1, Leuprorelin, Histrelin, Argiprestocin, Argipressin, F671-0144, F725-0072, E524-1708, L381-9578 and E852-1289 on the site 2 of the AC Chain.

On the Figure 4.1.14, 100 ns time dependent MM/GBSA scores of the Polymyxin B1, Leuprorelin, Histrelin, Argiprestocin, Argipressin, F671-0144, F725-0072, E524-1708, L381-9578 and E852-1289 on the site 2 of the AC Chain is shown. Histrelin molecule appear to have the highest negative MM/GBSA scores on the site 2 of the AC chain. Generally, MM/GBSA scores on this site accumulated between -60 and -120 kcal/mol.

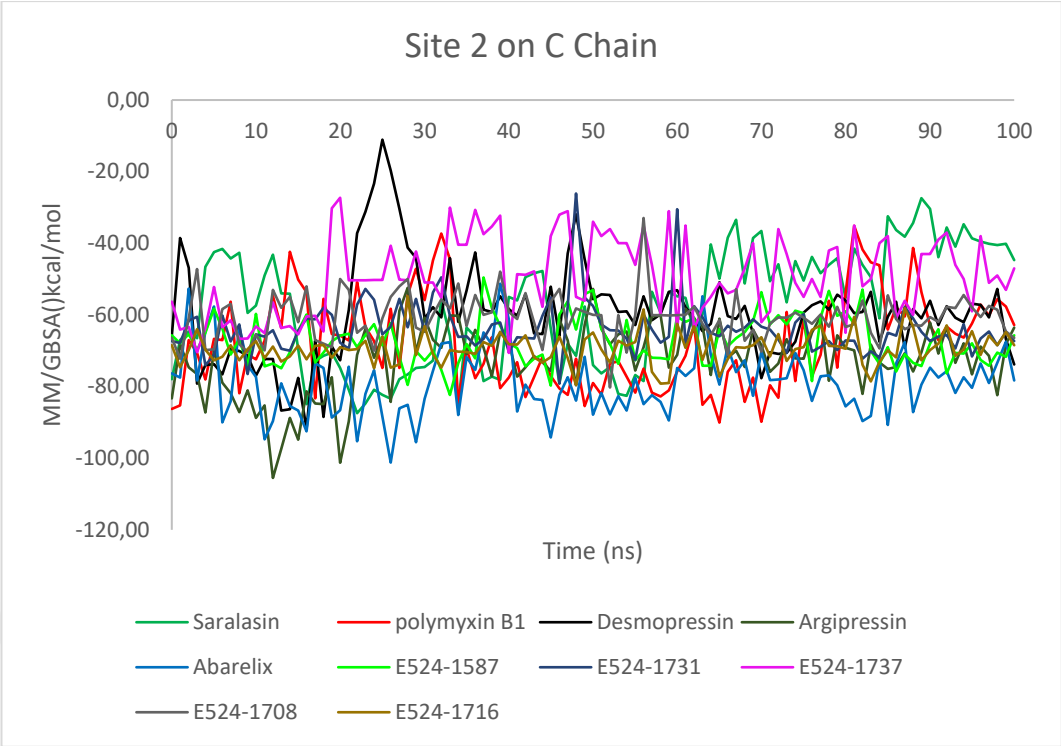

Figure 4.1.15. MM/GBSA-time graph of the Saralasin, Desmopressin, Polymyxin B1, Abarelix, Argipressin, E524-1587, E524-1731, E524-1737, E524-1708 and E524-1716 on the site 2 of the C Chain.

On the Figure 4.1.15, 100 ns time dependent MM/GBSA scores of the Polymyxin B1, Leuprorelin, Histrelin, Argiprestocin, Argipressin, E524-1587, E524-1731, E524-1737, E524-1708 and E524-1716 on the site 2 of the C Chain is shown. Abarelix molecule appear to have the highest negative MM/GBSA scores on the site 2 of the C chain. Generally, MM/GBSA scores on this site accumulated between -50 and -80 kcal/mol.

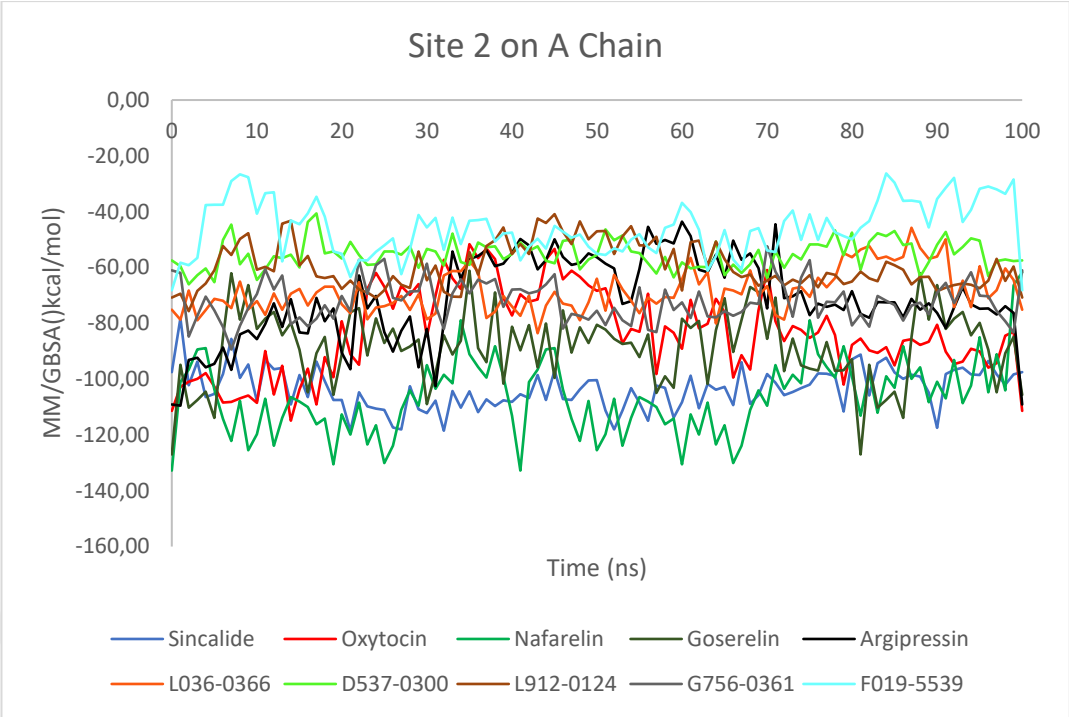

Figure 4.1.16. MM/GBSA-time graph of the Sincalide, Oxytocin, Nafarelin, Goserelin, Argipressin, L036-0366, D537-0300, L912-0124, G756-0361 and F019-5539 on the site 2 of the A Chain.

On the Figure 4.1.16, MM/GBSA scores depend on the 100 ns of the Sincalide, Oxytocin, Nafarelin, Goserelin, Argipressin, L036-0366, D537-0300, L912-0124, G756-0361 and F019-5539 on the site 2 of the A Chain is shown. F019-5539 has the lowest MM/GBSA scores than others and Nafarelin and Sincalide molecule appear to have the highest negative MM/GBSA score on the site 2 of the A chain.

4.2 Screening of Peptides

Besides screening of compounds from small molecule libraries, peptide sequences were also designed using interacted portions of the Gas6/Axl complex. The peptides were designed, and Glide/SP peptide docking calculations were conducted for all the designed peptides. For the high docking scored designed peptides, long (200 ns) MD simulations were performed. Simulations were repeated three times. Then, MM/GBSA calculations were performed to investigate the average binding free energies of the screened peptides. Table 4.4.1 represents docking scores and average MM/GBSA analyses from each run of the peptides.

Ten peptide sequences were designed and analyzed. All the designed peptides have a higher negative score than -100,00 kcal/mol. Also, the Glide/SP peptide docking scores of the peptides have high docking scores (i.e., >-9,00 kcal/mol). TPVIRLRFKR has the highest negative MM/GBSA score (-154,25 kcal/mol) and TPVIRLRFK has the highest negative Glide/SP docking score (-11,57 kcal/mol) (Table 4.4.1).

Table 4.4.1

The Glide SP docking scores and average MM/GBSA results of the designed peptides.

Peptide Sequences	Glide/SP Docking Score (kcal/mol)	MM/GBSA 200 ns (kcal/mol) #1	MM/GBSA 200 ns (kcal/mol) #2	MM/GBSA 200 ns (kcal/mol) #3	AVERAGE MM/GBSA (kcal/mol)
TPVIRLRFKR	-10,91	-154,65 ± 9,35	-153,83 ± 9,06	-154,26 ± 7,88	-154,25 ± 8,76
TPVIRLRFK	-11,57	-146,00 ± 6,70	-139,16 ± 15,95	-143,95 ± 8,86	-143,04 ± 10,5
PVIRLRFKR	-11,78	-141,28 ± 8,55	-133,05 ± 8,86	-143,57 ± 8,62	-139,30 ± 8,68
RLRFKRLQ	-9,36	-146,60 ± 17,40	-127,42 ± 34,29	-131,25 ± 12,92	-135,09 ± 22,36
VIRLRFKR	-11,40	-108,88 ± 18,84	-129,96 ± 11,93	-118,65 ± 14,17	-119,16 ± 14,98
PVIRLRFK	-10,04	-123,27 ± 9,00	-125,63 ± 8,92	-106,69 ± 12,04	-118,53 ± 9,97
IRLRFKR	-10,64	-124,99 ± 10,11	-104,05 ± 17,18	-120,73 ± 9,04	-116,59 ± 12,09
VIRLRFKRL	-10,62	-121,50 ± 12,07	-118,05 ± 14,14	-102,14 ± 15,93	-113,90 ± 14,05
IRLRFKRL	-10,82	-119,77 ± 10,69	-107,62 ± 8,88	-104,76 ± 11,83	-110,72 ± 10,47
VIRLRFK	-10,27	-105,25 ± 9,24	-109,21 ± 10,19	-100,40 ± 8,6	-104,95 ± 9,34

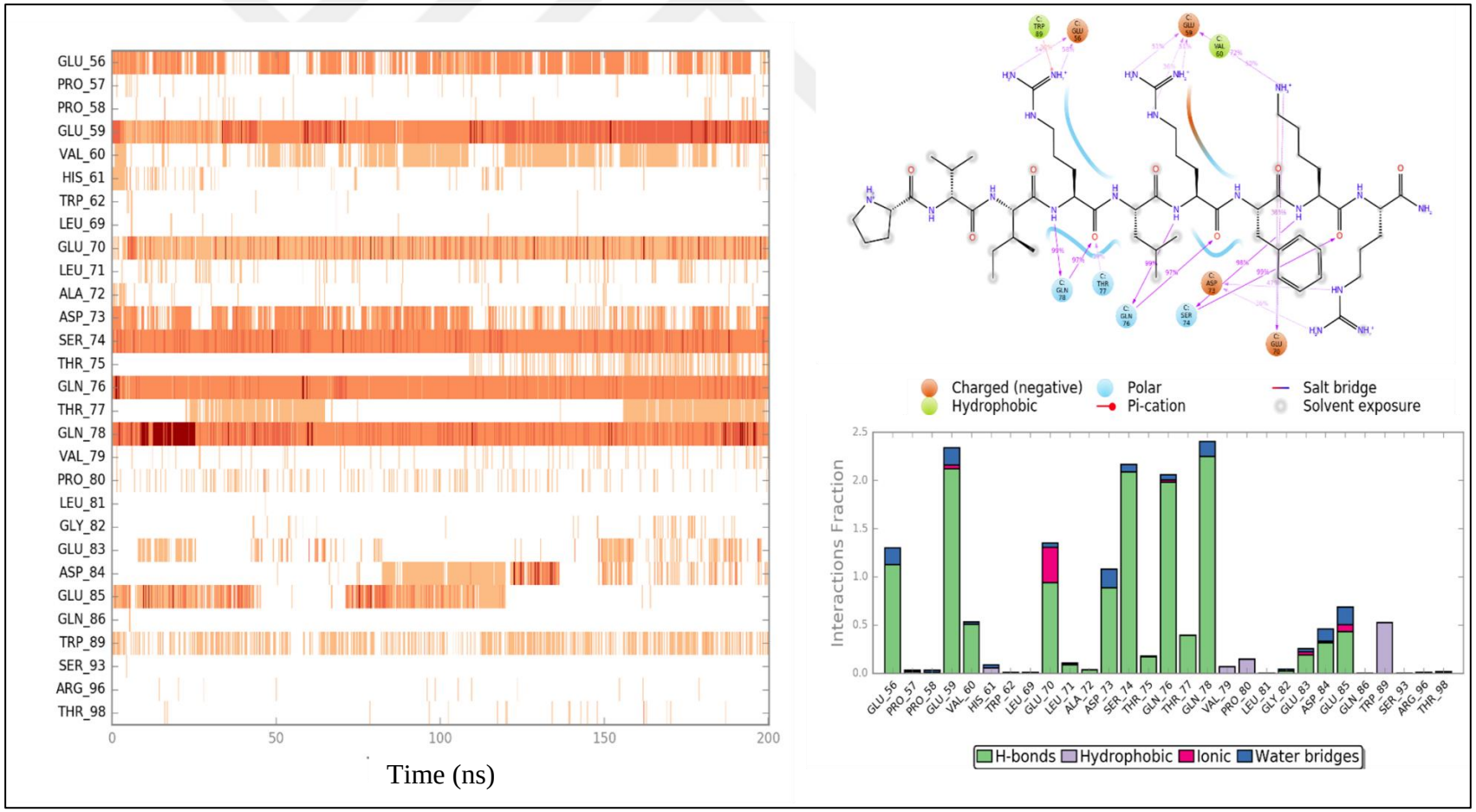

Figure 4.2.1. The interaction diagram of the PVIRLRFKR on the Axl protein during the 200 ns MD simulations.

The PVIRLRFKR peptide sequence is depicted (Figure 4.2.1). After the 200 ns MD simulations, representative frame was chosen using the nearest RMSD to the average RMSD. Glu59, Glu70, Ser74, Gln76, and Gln78 residues showed strong interactions during the 200 ns simulations. The peptide formed hydrogen bonds, hydrophobic interactions, water bridges, and ionic interactions with the protein. While Glu70, and Glu59 formed ionic interactions, and hydrogen bonds; Glu56, Asp73, Ser74, Gln76, and Gln78 formed hydrogen bonds and water bridges mainly. Gln78, Gln76, Ser74 interacted with the peptide more than ninety percent of the 200 ns simulation time.

In the Figure 4.2.2, representative frame of the 200 ns MD simulations of the PVIRLRFKR and Axl protein are depicted. The 3D ligand interaction diagram with the peptide at the cavity of binding site can be seen. On the representative frame, Ser447, and Gln459 formed H-bond interaction.

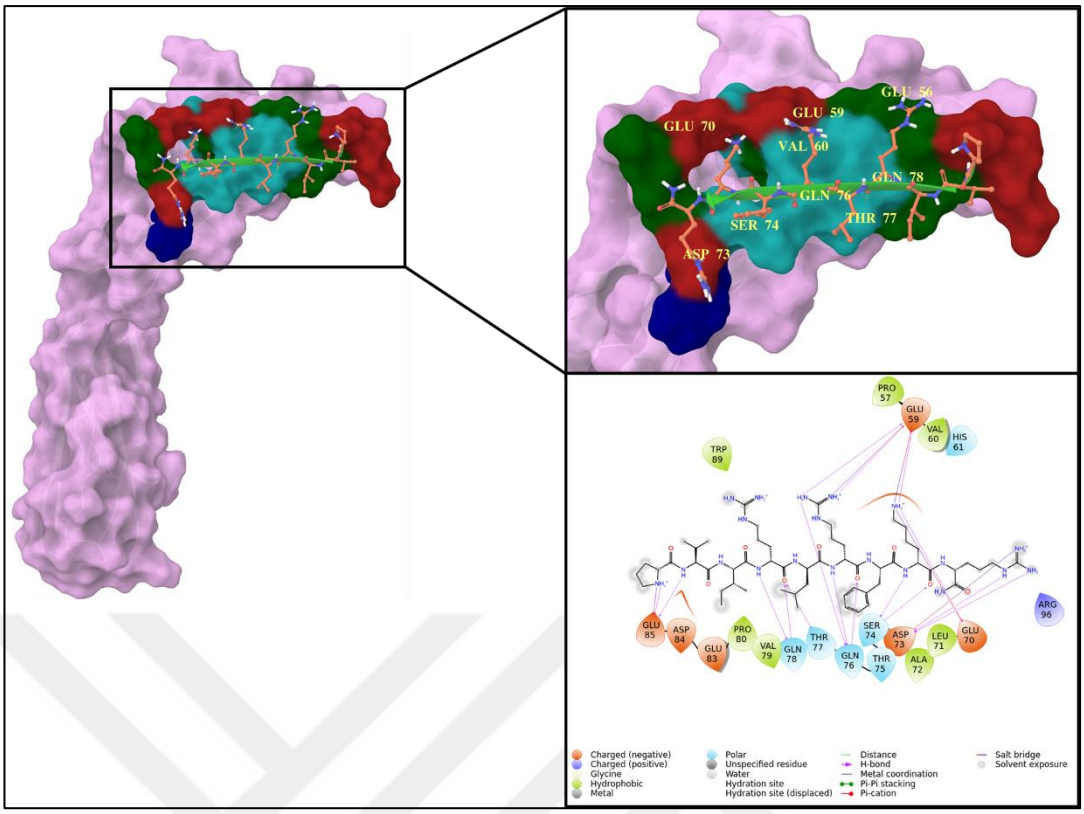

Figure 4.2.2. The representative frame of the 200 ns MD simulation of the PVIRLRFKR on the C chain.

4.2.1 The Secondary Structure Analysis of Peptides

VMD program was used to have graphs that shows the secondary structure of PVIRLRFK in *Figure 4.2.3*. The three MD simulations of the peptide sequence were concatenated. Yellow bands show extended β-sheet conformations, aqua bands show turns, white bands show no structure, and dark yellow bands show isolated bridges. A total of 3000 frames saved during the MD simulations from three independent runs. The peptide's secondary structure is visualized. While the extended structures, which forms the majority of the β sheet are depicted with yellow bands; turns, another β sheet component, are represented by aqua bands. The white bands are coils, indicating that there is no structure. Isolated bridges are depicted with dark yellow bands (Figure 4.2.3 - Figure 4.2.12). The β-sheet structure of Arg308, Leu309, Arg310, and Phe311 is usually protected (Figure 4.2.3). The turns, another component of β-sheet, are found in Pro305, Val306, and Ile307. On Arg308, there is a bridge formation between the 2361st and 2681st frames. Bridge formation was broken, and extended conformation was restored. Corresponding plots for PVIRLRFKR and RLRFKRLQ are represented at the Figure 4.2.4 and Figure 4.2.5.

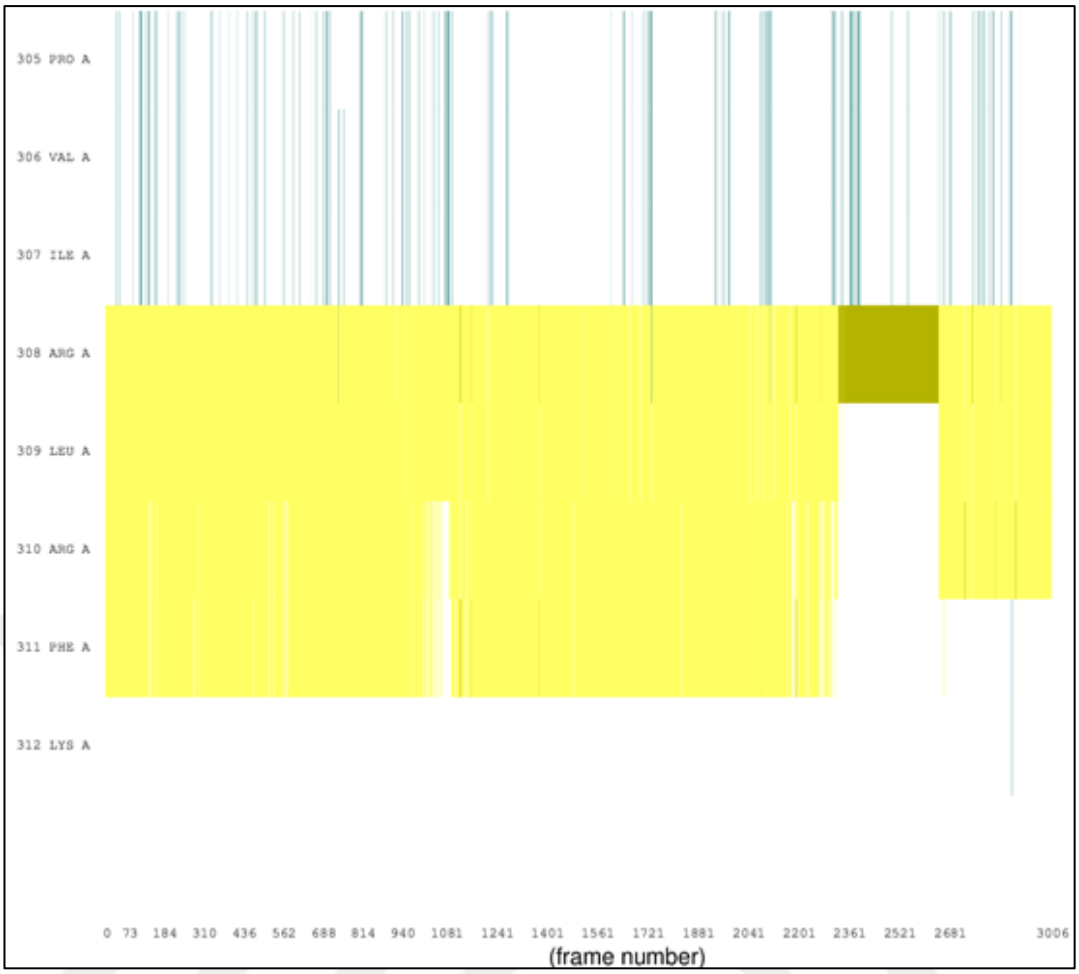

Figure 4.2.3. The secondary structure of PVIRLRFK.

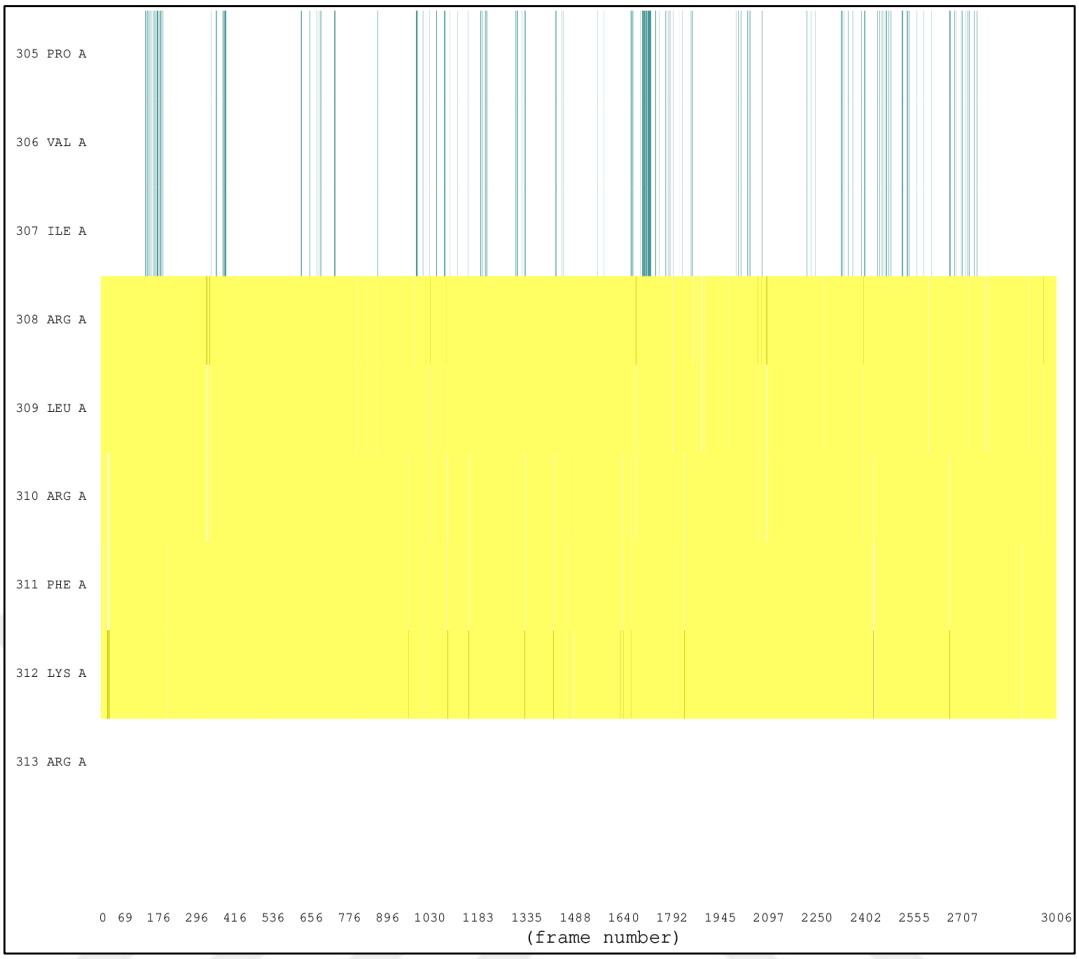

Figure 4.2.4. The secondary structure of PVIRLRFKR.

Figure 4.2.5. The secondary structure of RLRFKRLQ.

The secondary structure of the IRLRFKRL sequence is shown in Figure 4.2.6. After all frames of three MD simulations had been concatenated, these figures created (Figure 4.2.3 - Figure 4.2.12). Yellow bands show extended β-sheet conformations; aqua bands show turns; white bands show no structure, and dark yellow bands show isolated bridges. The β sheet of this peptide is shorter than that of other peptides. It did not entirely lose β-sheet. Lys312 is continually forming β sheets and bridges.

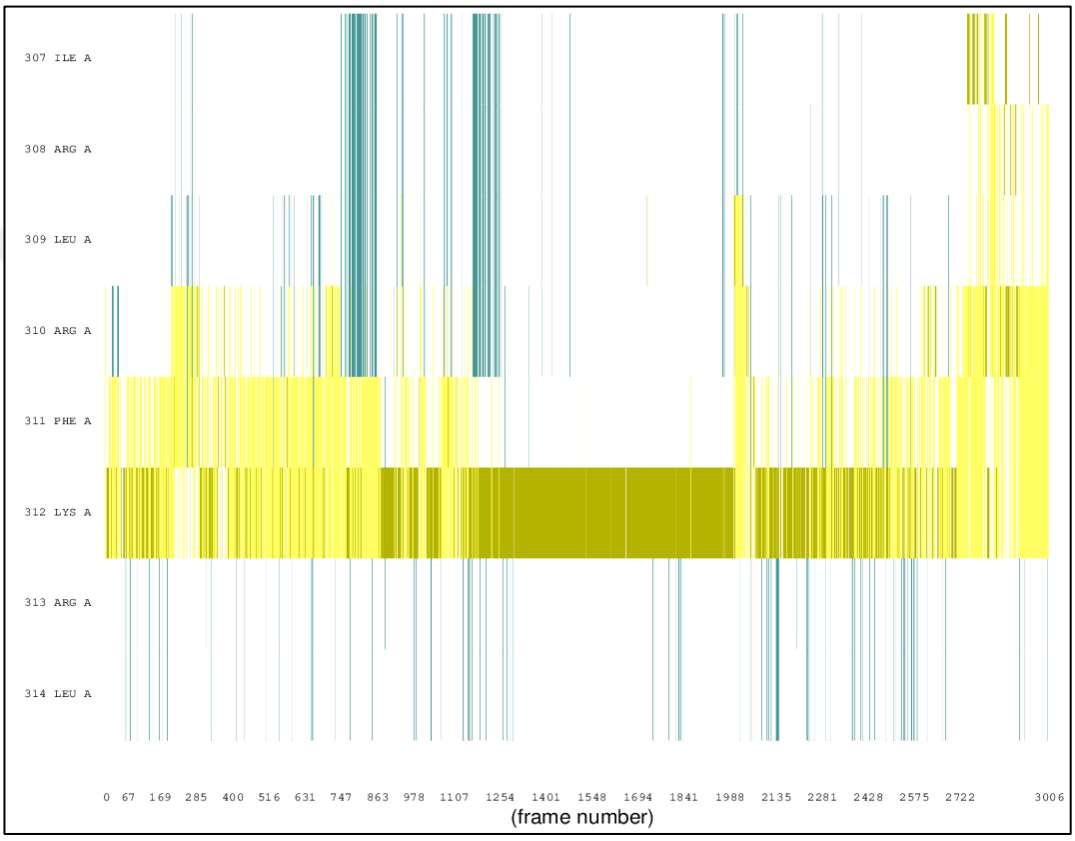

Figure 4.2.6. The secondary structure of IRLRFKRL.

The secondary structure of the IRLRFKR is seen in Figure 4.2.7. Because five of the residues (Arg308, Leu309, Arg310, Phe311, and Leu312) demonstrated extended β-sheet formation, this peptide has a longer β-sheet formation.

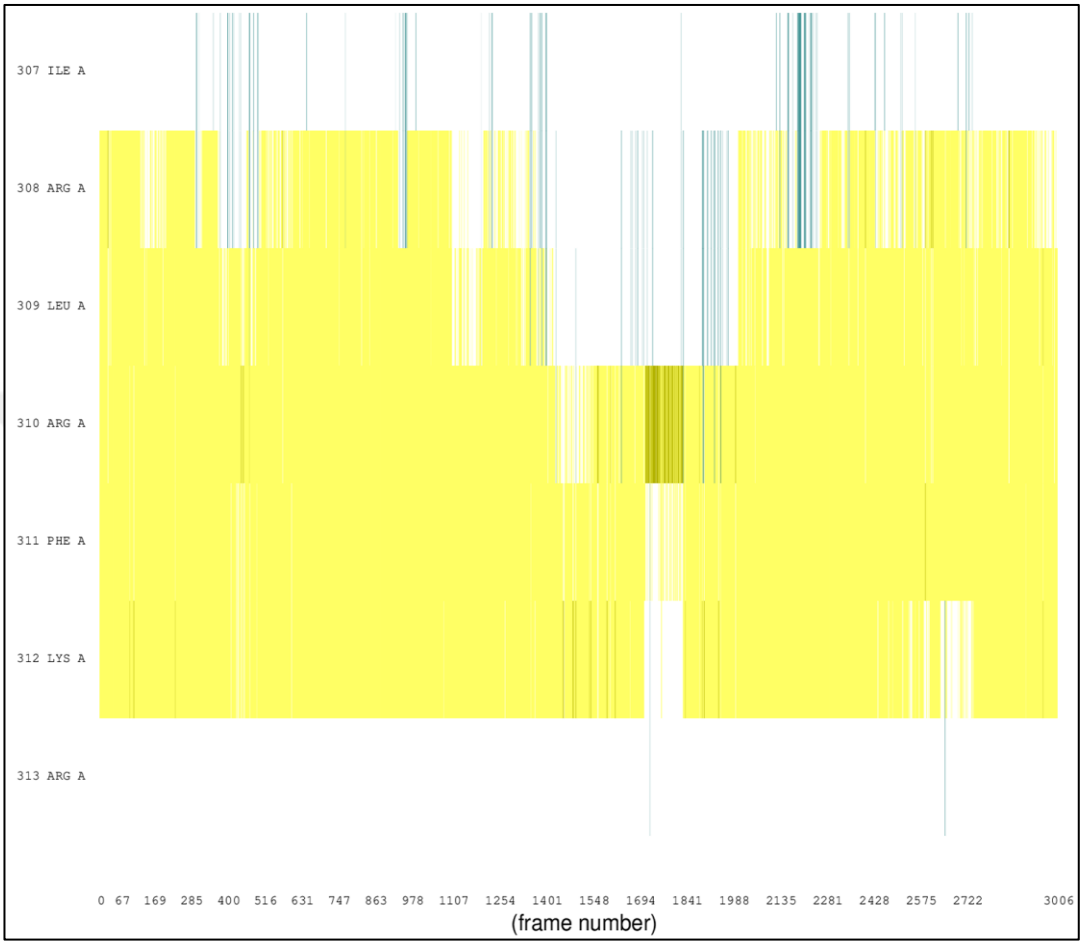

Figure 4.2.7. The secondary structure of IRLRFKR.

The secondary structure of the TPVIRLRFK is seen in Figure 4.2.8. In all three simulations, the Arg308, Leu309, Arg310, and Phe311forms β-sheet formation. Thr304, Pro305, Val306, and Ile307 include turns, another β-sheet formation, although Lys312 has no structure.

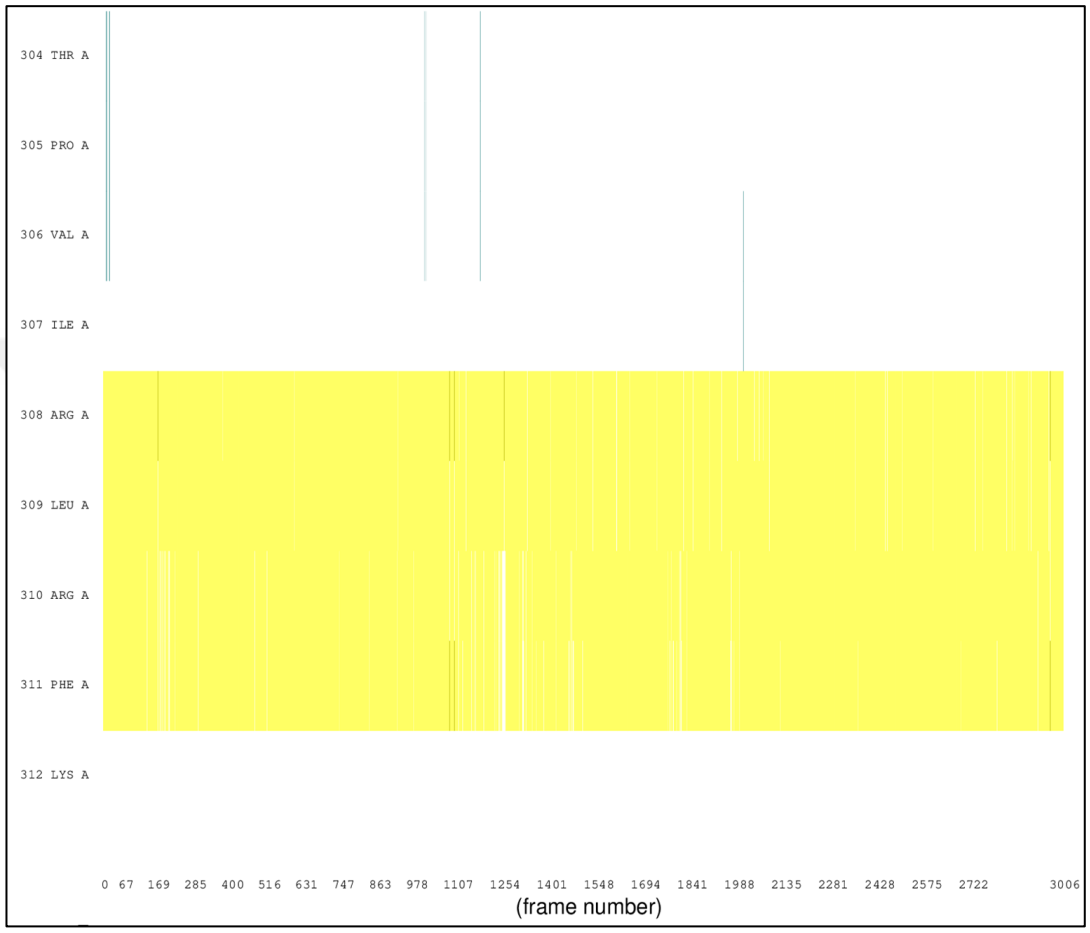

Figure 4.2.8. The secondary structure of TPVIRLRFK.

The secondary structure of the TPVIRLRFKR is seen in Figure 4.2.9. It has a similar formation to TPVIRLRFK, but Lys312 has an extended formation in TPVIRLRFKR.

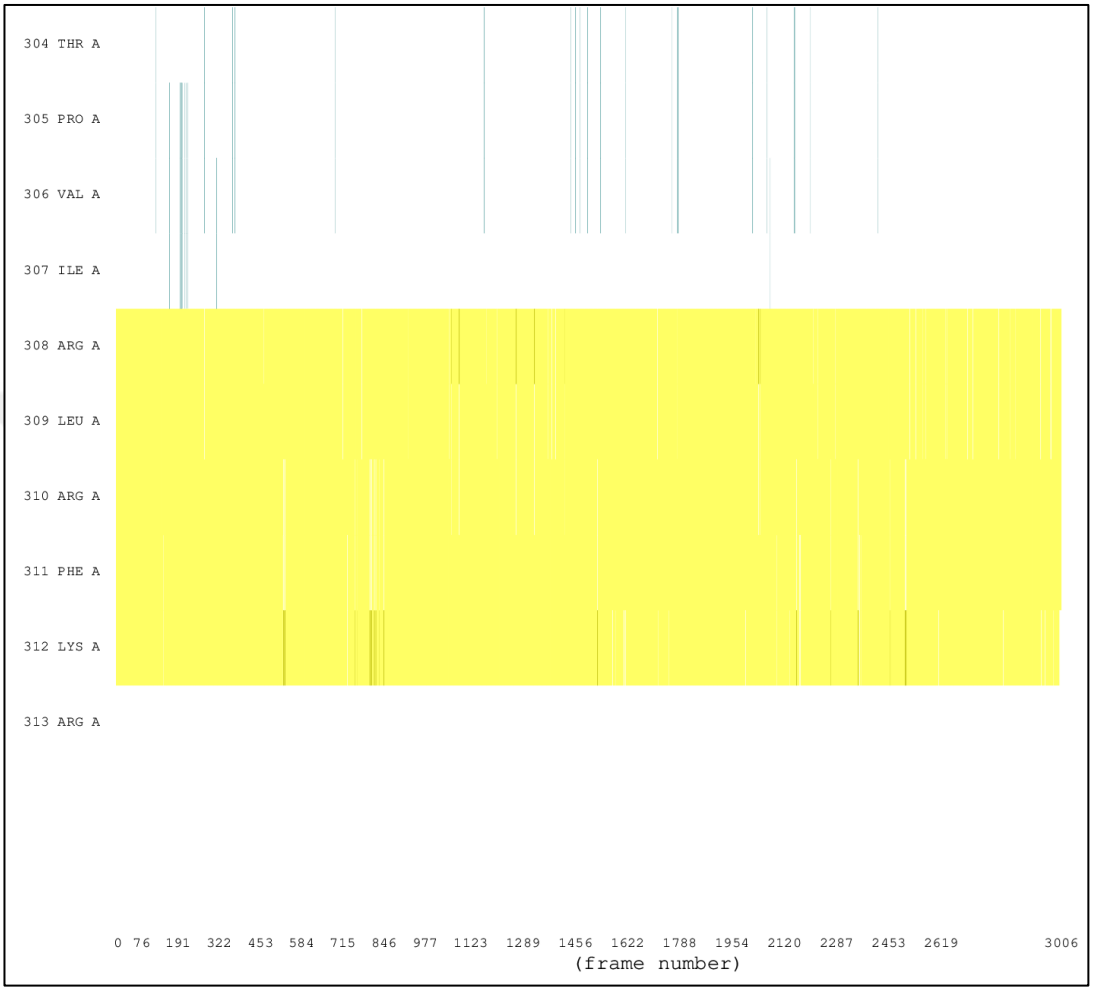

Figure 4.2.9. The secondary structure of TPVIRLRFKR.

The secondary structure of the VIRLRFKR is seen in Figure 4.2.10. There is the construction of a secondary structure, but it is not stable. For example, only the first 200 frames of Val306 include expanded sheets and bridges. During the simulation, Ile307, Arg308, Leu309, and Arg310 attempted to keep the secondary structure. Turns present in Phe311, Lys312, and Arg313.

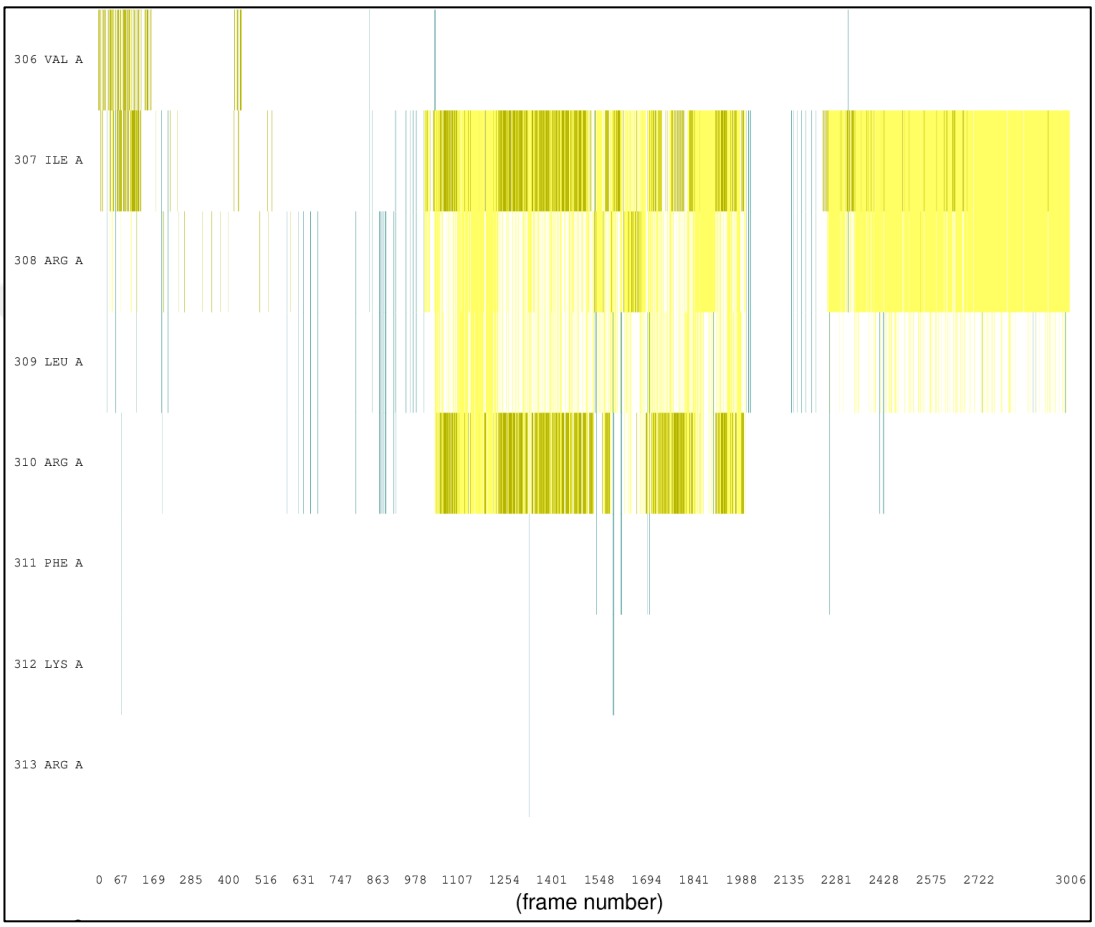

Figure 4.2.10. The secondary structure of VIRLRFKR.

The secondary structure of the VIRLRFKRL is seen in Figure 4.2.11. This peptide's secondary structure is maintained in all residues. There are few extended conformations and turns. There are turns on the Val306, Phe311, Lys312, Arg313, and Leu314, and extended conformation of sheets on the Ile307, Arg308, Leu309, and Arg310. Isolated bridges can be found on the Arg310 residue.

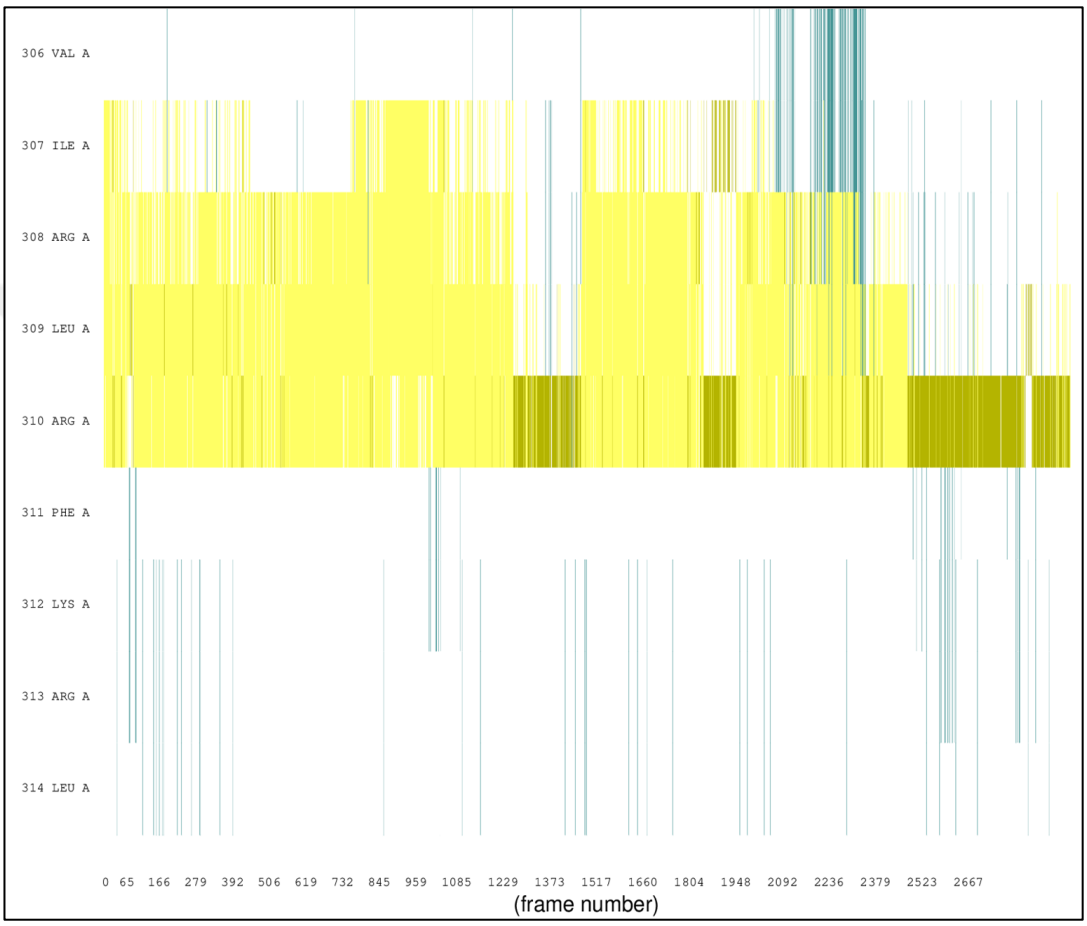

Figure 4.2.11. The secondary structure of VIRLRFKRL.

The secondary structure of VIRLRFK is seen in Figure 4.2.12. There are some turns and extended conformations in the Val306 and Ile307 regions. There is a β-sheet formation as well as bridges on the Arg308. There is a β-sheet formation on Leu309 and Arg310.

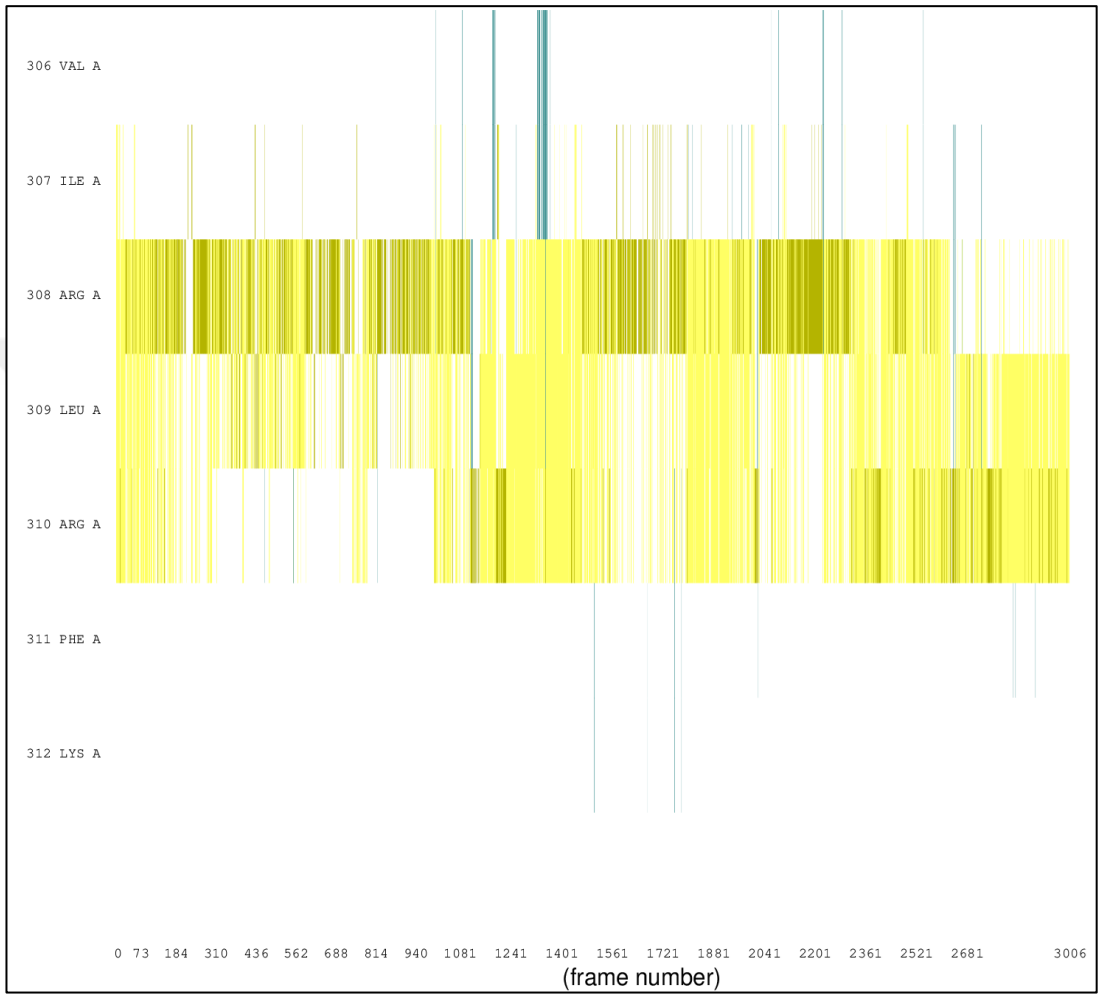

Figure 4.2.12. The secondary structure of VIRLRFK.

4.2.2 The MD simulations and MM/GBSA Analysis of Peptides

After 200 ns MD simulations, simulation interaction diagrams were created using Maestro molecular modeling package. Figure 4.2.13 shows the RMSD graph showing the deviations in the movement of the TPVIRLRFKR molecule on the target protein throughout the 200 ns MD simulations. While the blue colour shows the RMSD graph of the C alpha atoms of the protein, the red colour is the RMSD graph of the ligand (atoms other than hydrogen) relative to the protein. In both graphs, no large deviations from the initial structure were observed and the ligand did not diffuse the binding pocket and retained its interaction with the active site residues. This indicates that the ligand has strong interactions.

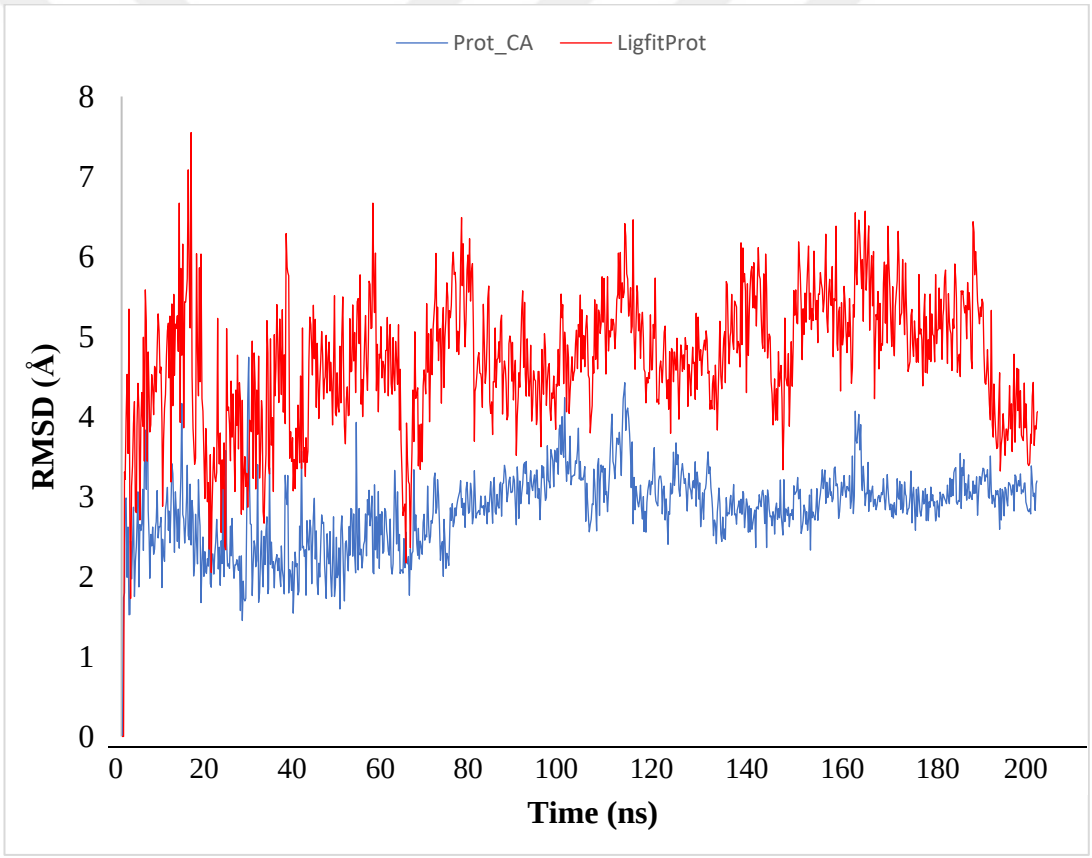

Figure 4.2.13. RMSD graph of the TPVIRLRFKR peptide sequence.

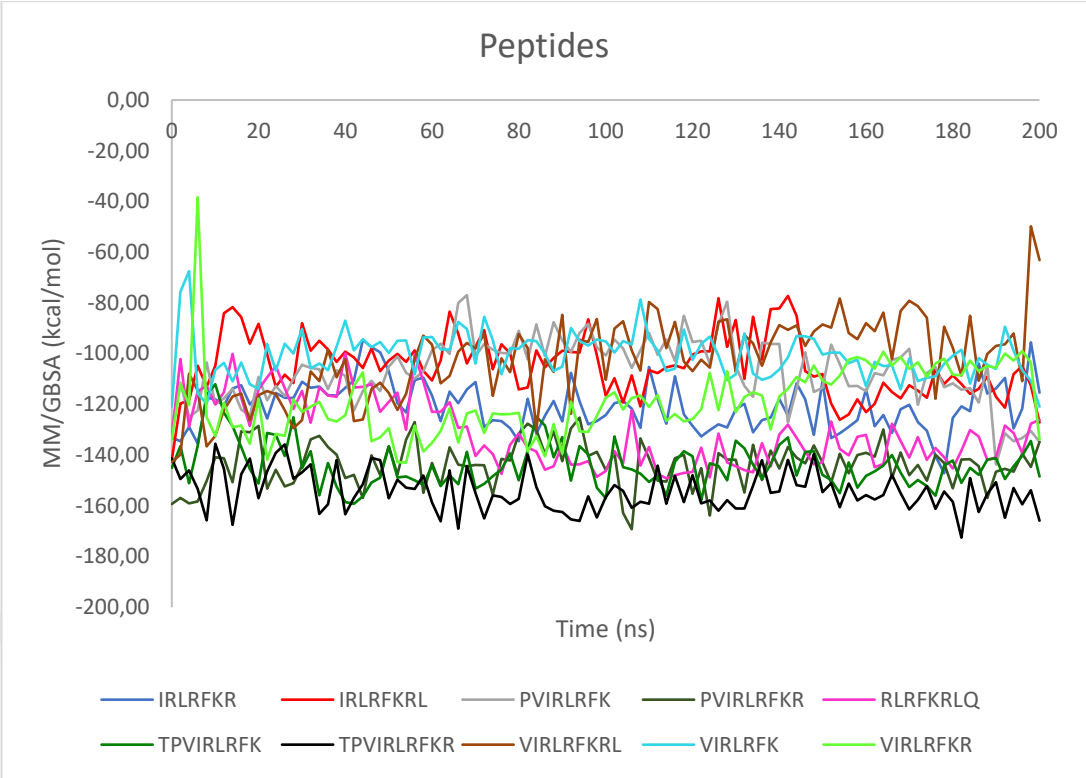

Figure 4.2.14. The MM/GBSA scores of the 200 ns MD simulation of ten peptide sequences on Axl target.

On the Figure 4.2.14, the MM/GBSA scores of the ten peptides can be seen. Target protein is Axl (C Chain). Ten peptide sequences are depicted as different colors. TPVIRLRFKR has the highest negative MM/GBSA score means that this sequence has stronger interactions than other sequences. Generally, peptides have strong interactions with the target protein. The MM/GBSA scores are between -100 and -160 kcal/mol.

Chapter 5

Discussions and Conclusions

One of the essential members of the TAM family is the Axl protein. Cell survival, migration, and proliferation are the main aim of the TAM protein family. Overexpression of the Axl and Gas6 proteins has been linked to a cancer prognosis (Axelrod and Pienta, 2014). When a patient is treated with chemotherapy medications, the cancer cells may become resistant to the cancer treatments. TAM receptor overexpression has been linked to cancer therapy resistance (Vouri and Hafizi, 2017; Falcone et al., 2020). Axl is overexpressed in medication-resistant cancer therapies. The Axl gene expression level is elevated in most cancer cell lines, such as kidney, breast cancer, and CNS (Hong et al., 2008). Therefore, it is critical to focus cancer research on the TAM family.

Other TAM family members, including Tyro3 and MerTK, have hydrophobic interface binding sites that are homologous. If these receptor kinase receptors can be controlled, the treatment could be more effective. They may become a major target in cancer treatment in the future. Therefore, our findings can be applied to other TAM protein family members (Kimani et al., 2017).

The study major goal is to find suitable inhibitory compounds for the Axl-Gas6 target. ChemDiv's peptidomimetic database and FDA-approved drugs and compounds in clinical investigation were virtually screened to identify the hit compounds which inhibits the Axl-Gas6 signalling pathway. On the Axl, there are multiple druggable sites; however, only two of them (located on the protein's extracellular domain) were studied in the study. When Gas6 is coupled to Axl on the extracellular cell surface, a hydrophobic contact forms inside the cavity. One of the druggable locations is this cavity. In Axl, the residues around the hydrophobic interface are Thr46, Thr77, Val92, Gln94, and Arg96; in Gas6, the residues around the hydrophobic interface are 446-459, Ile307, Leu309, Phe311, Thr461, and Met468. Kimani et al. searched for small molecule inhibitors that target the hydrophobic interface in their study. Small compounds known as RU-301 and RU-302 are potent inhibitors of the Axl target. They focused on the extracellular component, and the small compounds were effective at

inhibiting Axl-Gas6 signalling. On the hydrophobic interface binding site (site 1), RU-301 and RU-302 molecules are used as reference molecules in our study. When peptidomimetics binds to Gas6's site 1, two molecules (G842-0689 and F723-0087) have found a significantly higher negative MM/GBSA score than RU-301, but RU-302 has a lower negative MM/GBSA score than the five other peptidomimetics.

The site 1 binding pocket is largely engaged on the Gas6 protein (A chain), therefore, MM/GBSA scores for Axl protein (C chain) binding lower negative than -50 kcal/mol. The highest negative MM/GBSA binding score belongs to Pentagastrin molecule on the site 1 of the C chain (Table 4.1.2). Oher small molecules have lower MM/GBSA scores than -50 kcal/mol (also in Figure 4.1.12). On the site 2, Abarelix molecule has the highest negative MM/GBSA score (-92,12 kcal/mol) (Table 4.1.2). Other molecules have MM/GBSA scores in the range of -50 and -80 kcal/mol (Figure 4.1.15).

On the AC chain, the Axl-Gas6 protein complex is bound. Therefore, the site 1 and site 2 binding sites are on both. On site 1, Saquinavir molecule has the highest negative MM/GBSA score (-90,62 kcal/mol) (Table 4.1.3). Saquinavir has strong interactions. Trp448 and Gln459 residues showed strong binding throughout the 100 ns MD simulation. The important residues on the binding pocket are Gln459 and Ser447. Saquinavir formed hydrogen bonds and water bridges with Ser447 and Gln459 (Figure 4.1.8 and Figure 4.1.9). Also, in the RMSD graph, no large deviations from the initial structure were observed and the ligand did not diffuse the binding pocket and retained its interaction with the active site residues. This indicates that the ligand has strong interactions (Figure 4.1.10). The MM/GBSA scores for small molecules are in between -60 and -90 kcal/mol (Figure 4.1.11). On the site 2, Histrelin has the highest negative MM/GBSA score (-108,42 kcal/mol). Leuprorelin, Argiprestocin, Polymyxin B1, Argipressin also has higher negative MM/GBSA scores than -70 kcal/mol (Table 4.1.3).

A chain is the Gas6 protein alone. When Gas6 is alone it is not bound on the receptor protein. The chosen binding sites interfere with the Axl binding; therefore, it will prevent Axl binding. On site 1, G842-0689 has the highest negative MM/GBSA binding score (-88,89 kcal/mol) (Table 4.1.1). F723-0087 also has -86,78 kcal/mol

average MM/GBSA score. The average MM/GBSA scores are in between -60 and -100 kcal/mol (Figure 4.1.16). on the site 2, Nafarelin has the highest MM/GBSA score (-97,32 kcal/mol) (Table 4.1.1). Sincalide, Goserelin, Oxytocin and Argipressin also has the strong interactions.

In addition, ten peptides were designed to target Axl and compete with Gas6 binding. The Maestro Molecular Modeling program was used to create peptides that mimicked the Gas6 binding on the site 2. The β-sheet of the Gas6 protein that interacts with Axl was truncated (TPVIRLRFKRLQ), keeping key residues including Arg308, Arg310, and Lys312 (Sasaki et al., 2006). Ten peptides with 7-10 amino acids were created around these residues, and molecular docking simulations were initiated after preparing peptides. The peptides have strong interactions with the site 2 of the C chain. Ten peptides have higher negative docking score than -10 kcal/mol (Table 4.4.1). After 200 ns MD simulations, the interaction diagram of the PVIRLRFKR sequence is seen in Figure 4.2.2. Glu59, Glu70, Ser74, Gln76, and Gln78 residues showed strong binding contacts throughout the 200 ns simulations. Gln78, Gln76, Ser74 resides interacted with the peptide more than ninety percent of the 200 ns simulation time (Figure 4.2.1). Also, other peptides have similar scores and similar diagrams. The binding pocket of the site 2 on the C chain can be seen in Figure 4.2.2. The peptide formed hydrogen bonds with Ser447 and Gln459 residues.

During 200 ns simulations, H-bonds, ionic bonds, water bridges, and many hydrophobic interactions are formed. Glu56 and Glu59 are the fundamental interactions that must be kept steady throughout MD simulations. The MM/GBSA calculations of the peptides are provided in Table 4.4.1. TPVIRLRFKR sequence has the highest negative binding energy as MM/GBSA average binding energy of -154,25 kcal/mol. For this peptide, the MD simulation repeats are also consistent. Figure 4.2.2 shows 200-ns MD simulations of the PVIRLRFKR on site 2 of C chain. Glu56, Glu59, Glu70, Ser74, Gln76, and Gln78 residues had strong interactions throughout the 200 ns MD simulations. Glu56 residue formed hydrogen bond and a water bridge; Glu59 formed hydrogen bonds, ionic bonds, and water bridges interactions. Also, other residues have strong interactions with the peptide (Figure 4.2.1). Even though its MM/GBSA scored of RLRFKRLQ sequence are found high, it is fluctuated at the

binding pocket during the simulations. The crucial point about peptide design is to check if the peptides preserve their secondary structure during MD simulations. The trimmed part of the Gas6 protects its β-sheet structure; therefore, it is important that the peptide sequences preserve their β-sheet conformation during 200 ns MD simulations. As a result, the peptides' secondary structures remain stable during simulations. Overall, the β-sheet structure is stable and intact (Figure 4.2.3 - Figure 4.2.12).

Xing et al. investigated the use of peptides derived from snake venom to prevent Zika virus (ZIKV) infection. They focused on the Axl-Socs (cytokine signalling protein suppressor) pathway. The peptides extracted from the venom had anti-ZIKV action and could also be used to treat other viral infections (Xing et al., 2020). The Axl-Gas6 proteins are also involved in viral infection.

The N-terminal domain of the SARS-CoV-2 Spike protein interacts with Axl. Morales et al. found that the plasma Gas6 level increased in COVID-19 patients and the increase is related to the severity of the disease (Morales et al., 2021). Overexpression of the Axl creates the similar effect as overexpression of the ACE2 receptor (Leelananda and Lindert, 2016). As a result, Axl-Gas6 is a critical target for both cancer and viral infections. Peptide design may pave the way for future use as an Axl-Gas6 signalling inhibitor to treat cancer and viral infections.

In conclusion, the hit molecules from peptidomimetics and FDA libraries can be used as an inhibitor on the Axl-Gas6 protein complex, and ten peptides can be used as peptide-based inhibitors as mimicking the Gas6 binding on the Axl. The obtained hit compounds against Gas6/Axl protein complex need to be validated by in vitro experiments before considering them at the further preclinical investigations.

REFERENCES

Books

Cramer, Christopher J., Horn, A. H. C. (2003). Essentials of Computational Chemistry, Theories and Models By Christopher J. Cramer, Journal of Chemical Information and Computer Sciences. doi: 10.1021/ci010445m

Periodicals

Anderson, H. A. et al. (2003) 'Serum-derived protein S binds to phosphatidylserine and stimulates the phagocytosis of apoptotic cells.', Nature immunology, 4(1), pp. 87–91. doi: 10.1038/ni871.

Angelillo-Scherrer, A et al. (2001) 'Deficiency or inhibition of Gas6 causes platelet dysfunction and protects mice against thrombosis.', Nature medicine, 7(2), pp. 215–221. doi: 10.1038/84667.

Axelrod, H. and Pienta, K. J. (2014) 'Axl as a mediator of cellular growth and survival', Oncotarget, 5(19), pp. 8818–8852. doi: 10.18632/oncotarget.2422.

Behrens, E. M. et al. (2003) 'The mer receptor tyrosine kinase: expression and function suggest a role in innate immunity.', European journal of immunology, 33(8), pp. 2160–2167. doi: 10.1002/eji.200324076.

Bellosta, P. et al. (1995) 'The receptor tyrosine kinase ARK mediates cell aggregation by homophilic binding.', Molecular and Cellular Biology, 15(2), pp. 614–625. doi: 10.1128/mcb.15.2.614.

Chen, J., Carey, K. and Godowski, P. J. (1997) 'Identification of Gas6 as a ligand for Mer, a neural cell adhesion molecule related receptor tyrosine kinase implicated in cellular transformation.', Oncogene, 14(17), pp. 2033–2039. doi: 10.1038/sj.onc.1201039.

Cohen, P. L. et al. (2002) 'Delayed apoptotic cell clearance and lupus-like autoimmunity in mice lacking the c-mer membrane tyrosine kinase.', The Journal of experimental medicine, 196(1), pp. 135–140. doi: 10.1084/jem.20012094.

Cramer, Christopher J., Horn, A. H. C. (2003) Essentials of Computational Chemistry, Theories and Models By Christopher J. Cramer, Journal of Chemical Information and Computer Sciences. doi: 10.1021/ci010445m.

Craven, R. J. et al. (1995) 'Receptor tyrosine kinases expressed in metastatic colon cancer.', International journal of cancer, 60(6), pp. 791–797. doi: 10.1002/ijc.2910600611.

Crosier, P. S. et al. (1995) 'Identification of a novel receptor tyrosine kinase expressed in acute myeloid leukemic blasts.', Leukemia & lymphoma, 18(5–6), pp. 443–

449. doi: 10.3109/10428199509059643.

Dahlbäck, B. and Villoutreix, B. O. (2005) 'Regulation of blood coagulation by the protein C anticoagulant pathway: novel insights into structure-function relationships and molecular recognition.', Arteriosclerosis, thrombosis, and vascular biology, 25(7), pp. 1311–1320. doi: 10.1161/01.ATV.0000168421.13467.82.

Falcone, I. et al. (2020) 'AXL receptor in breast cancer: Molecular involvement and therapeutic limitations', International Journal of Molecular Sciences, 21(22), pp. 1–23. doi: 10.3390/ijms21228419.

Fisher, P. W. et al. (2005) 'A novel site contributing to growth-arrest-specific gene 6 binding to its receptors as revealed by a human monoclonal antibody.', The Biochemical journal, 387(Pt 3), pp. 727–735. doi: 10.1042/BJ20040859.

Godowski, P. J. et al. (1995) 'Reevaluation of the roles of protein S and Gas6 as ligands for the receptor tyrosine kinase Rse/Tyro 3.', Cell, 82(3), pp. 355–358. doi: 10.1016/0092-8674(95)90424-7.

Guttridge, K. L. et al. (2002) 'Mer Receptor Tyrosine Kinase Signaling: Prevention of Apoptosis and Alteration of cytoskeletal architecture without stimulation or proliferation', Journal of Biological Chemistry, 277(27), pp. 24057–24066. doi: 10.1074/JBC.M112086200.

Hangs, B. S. K. and Quinn, A. M. (1991) 'Protein Kinase Catalytic Domain Sequence Database: Identification of Conserved Features of Primary Structure and Classification of Family Members', Methods Enzymol, 200(1987), pp. 38–62. doi: 10.1016/0076-6879(91)00126-h.

Heldin, C. H. (1995) 'Dimerization of cell surface receptors in signal transduction', Cell, 80(2), pp. 213–223. doi: 10.1016/0092-8674(95)90404-2.

Holland, S. J. et al. (2010) 'R428, a selective small molecule inhibitor of Axl kinase, blocks tumor spread and prolongs survival in models of metastatic breast cancer', Cancer Research, 70(4), pp. 1544–1554. doi: 10.1158/0008-5472.CAN-09-2997.

Hong, C. C. et al. (2008) 'Receptor tyrosine kinase AXL is induced by chemotherapy drugs and overexpression of AXL confers drug resistance in acute myeloid leukemia', Cancer Letters, 268(2), pp. 314–324. doi:

10.1016/j.canlet.2008.04.017.

Hu, B. et al. (2004) ‘Resident murine alveolar and peritoneal macrophages differ in adhesion of apoptotic thymocytes.’, American journal of respiratory cell and molecular biology, 30(5), pp. 687–693. doi: 10.1165/rcmb.2003-0255OC.

Ishimoto, Y. et al. (2000) ‘Promotion of the uptake of PS liposomes and apoptotic cells by a product of growth arrest-specific gene, gas6.’, Journal of biochemistry, 127(3), pp. 411–417. doi: 10.1093/oxfordjournals.jbchem.a022622.

Jacob, A. N. et al. (1999) ‘A receptor tyrosine kinase, UFO/Axl, and other genes isolated by a modified differential display PCR are overexpressed in metastatic prostatic carcinoma cell line DU145.’, Cancer detection and prevention, 23(4), pp. 325–332. doi: 10.1046/j.1525-1500.1999.99034.x.

Jia, R. et al. (1992) ‘A novel oncogene, v-ryk, encoding a truncated receptor tyrosine kinase is transduced into the RPL30 virus without loss of viral sequences.’, Journal of virology, 66(10), pp. 5975–5987. doi: 10.1128/JVI.66.10.5975-5987.1992.

Katagiri, M. et al. (2001) ‘Mechanism of stimulation of osteoclastic bone resorption through Gas6/Tyro 3, a receptor tyrosine kinase signaling, in mouse osteoclasts.’, The Journal of biological chemistry, 276(10), pp. 7376–7382. doi: 10.1074/jbc.M007393200.

Kimani, S. G. et al. (2017) ‘Small molecule inhibitors block Gas6-inducible TAM activation and tumorigenicity’, Scientific Reports. doi: 10.1038/srep43908.

Lai, C. and Lemke, G. (1991) ‘An extended family of protein-tyrosine kinase genes differentially expressed in the vertebrate nervous system’, Neuron, 6(5), pp. 691–704. doi: 10.1016/0896-6273(91)90167-X.

Leelananda, S. P. and Lindert, S. (2016) ‘Computational methods in drug discovery’, Beilstein Journal of Organic Chemistry, 12, pp. 2694–2718. doi: 10.3762/bjoc.12.267.

Lemke, G. and Lu, Q. (2003) ‘Macrophage regulation by Tyro 3 family receptors.’, Current opinion in immunology, 15(1), pp. 31–36. doi: 10.1016/s0952-7915(02)00016-x.

Lewis, P. M. et al. (1996) ‘Analysis of the murine Dtk gene identifies conservation of genomic structure within a new receptor tyrosine kinase subfamily’, Genomics,

31(1), pp. 13–19. doi: 10.1006/geno.1996.0003.

Linger, R. M. A. et al. (2008) ‘TAM Receptor Tyrosine Kinases: Biologic Functions, Signaling, and Potential Therapeutic Targeting in Human Cancer’, Advances in Cancer Research, 100(08), pp. 35–83. doi: 10.1016/S0065-230X(08)00002-X.

Liu, E., Hjelle, B. and Bishop, J. M. (1988) ‘Transforming genes in chronic myelogenous leukemia.’, Proceedings of the National Academy of Sciences of the United States of America, 85(6), p. 1952. doi: 10.1073/PNAS.85.6.1952.

Lu, Q. et al. (1999) ‘Tyro-3 family receptors are essential regulators of mammalian spermatogenesis.’, Nature, 398(6729), pp. 723–728. doi: 10.1038/19554.

Lu, Q. and Lemke, G. (2001) ‘Homeostatic regulation of the immune system by receptor tyrosine kinases of the Tyro 3 family.’, Science (New York, N.Y.), 293(5528), pp. 306–311. doi: 10.1126/science.1061663.

Mahajan, N. P. et al. (2005) ‘Activated tyrosine kinase Ack1 promotes prostate tumorigenesis: role of Ack1 in polyubiquitination of tumor suppressor Wwox.’, Cancer research, 65(22), pp. 10514–10523. doi: 10.1158/0008-5472.CAN-05-1127.

Mark, M. R. et al. (1996) ‘Characterization of Gas6, a member of the superfamily of G domain-containing proteins, as a ligand for Rse and Axl’, Journal of Biological Chemistry. doi: 10.1074/jbc.271.16.9785.

Mark, M. R. et al. (1994) ‘rse, a Novel Receptor-type Tyrosine Kinase with Homology to AxVUfo, Is Expressed at High Levels in the Brain’, Journal of Biological Chemistry, 269(14), pp. 10720–10728. doi: 10.1016/S0021-9258(17)34118-2.

McCloskey, P. et al. (1997) ‘GAS6 mediates adhesion of cells expressing the receptor tyrosine kinase Axl.’, The Journal of biological chemistry, 272(37), pp. 23285–23291. doi: 10.1074/jbc.272.37.23285.

Morales, A. et al. (2021) ‘Growth arrest-specific factor 6 (Gas6) is increased in covid-19 patients and predicts clinical outcome’, Biomedicines, 9(4), pp. 1–11. doi: 10.3390/biomedicines9040335.

Nagata, K. et al. (1996) ‘Identification of the product of growth arrest-specific gene 6 as a common ligand for Axl, Sky, and Mer receptor tyrosine kinases.’, The Journal of biological chemistry, 271(47), pp. 30022–30027. doi: 10.1074/jbc.271.47.30022.

Nakano, T. et al. (1997) ‘Cell adhesion to phosphatidylserine mediated by a product of growth arrest-specific gene 6.’, The Journal of biological chemistry, 272(47), pp. 29411–29414. doi: 10.1074/jbc.272.47.29411.

Neubauer, Andreas et al. (1994) ‘Expression of axl, a transforming receptor tyrosine kinase, in normal and malignant hematopoiesis’, Blood, 84(6), pp. 1931–1941. doi: 10.1182/blood.v84.6.1931.1931.

O’Bryan, J. P. et al. (1991) ‘Axl, a Transforming Gene Isolated From Primary Human Myeloid Leukemia Cells, Encodes a Novel Receptor Tyrosine Kinase.’, Molecular and Cellular Biology, 11(10), pp. 5016–5031. doi: 10.1128/mcb.11.10.5016.

Olsson, M.H.M. et al. (2011) 'Propka3: Consistent Treatment of Internal and Surface Residues in Empirical pKa Predictions' Journal of Chemical Theory and Computation 7 (2), pp. 525-537.doi: 10.1021/ct100578z

Prasad, D. et al. (2006) ‘TAM receptor function in the retinal pigment epithelium.’, Molecular and cellular neurosciences, 33(1), pp. 96–108. doi: 10.1016/j.mcn.2006.06.011.

Robinson, D. R., Wu, Y. M. and Lin, S. F. (2000) ‘The protein tyrosine kinase family of the human genome’, Oncogene, 19(49), pp. 5548–5557. doi: 10.1038/sj.onc.1203957.

Rochlitz, C. et al. (1999) ‘Axl expression is associated with adverse prognosis and with expression of Bcl-2 and CD34 in de novo acute myeloid leukemia (AML): results from a multicenter trial of the Swiss Group for Clinical Cancer Research (SAKK).’, Leukemia, 13(9), pp. 1352–1358. doi: 10.1038/sj.leu.2401484.

Sainaghi, P. P. et al. (2005) ‘Gas6 induces proliferation in prostate carcinoma cell lines expressing the Axl receptor.’, Journal of cellular physiology, 204(1), pp. 36–44. doi: 10.1002/jcp.20265.

Sarukhanyan, E., Shityakov, S. and Dandekar, T. (2018) ‘In Silico Designed Axl Receptor Blocking Drug Candidates Against Zika Virus Infection’, ACS Omega, 3(5), pp. 5281–5290. doi: 10.1021/acsomega.8b00223.

Sarukhanyan, E., Shityakov, S. and Dandekar, T. (2020) ‘Rational Drug Design of Axl Tyrosine Kinase Type I Inhibitors as Promising Candidates Against Cancer’, Frontiers in Chemistry, 7(February), pp. 1–17. doi: 10.3389/fchem.2019.00920.

Sasaki, T. et al. (2002a) ‘Crystal structure of a C-terminal fragment of growth arrest-specific protein Gas6: Receptor tyrosine kinase activation by laminin G-like domains’, Journal of Biological Chemistry, 277(46), pp. 44164–44170. doi: 10.1074/jbc.M207340200.

Sasaki, T. et al. (2002b) ‘Crystal structure of a C-terminal fragment of growth arrest-specific protein Gas6: Receptor tyrosine kinase activation by laminin G-like domains’, Journal of Biological Chemistry, 277(46), pp. 44164–44170. doi: 10.1074/jbc.M207340200.

Sasaki, T. et al. (2006) ‘Structural basis for Gas6-Axl signalling’, EMBO Journal. doi: 10.1038/sj.emboj.7600912.

Sather, S. et al. (2007) ‘A soluble form of the Mer receptor tyrosine kinase inhibits macrophage clearance of apoptotic cells and platelet aggregation’, Blood
., doi: 10.1182/blood-2006.

Scott, R. S. et al. (2001) ‘Phagocytosis and clearance of apoptotic cells is mediated by MER.’, Nature, 411(6834), pp. 207–211. doi: 10.1038/35075603.

Seitz, H. M. et al. (2007) ‘Macrophages and dendritic cells use different Axl/Mertk/Tyro3 receptors in clearance of apoptotic cells.’, Journal of immunology (Baltimore, Md. : 1950), 178(9), pp. 5635–5642. doi: 10.4049/jimmunol.178.9.5635.

Shieh, Y.-S. et al. (2005) ‘Expression of axl in lung adenocarcinoma and correlation with tumor progression.’, Neoplasia (New York, N.Y.), 7(12), pp. 1058–1064. doi: 10.1593/neo.05640.

Son, M. Y. et al. (2014) ‘Comparative receptor tyrosine kinase profiling identifies a novel role for AXL in human stem cell pluripotency’, Human molecular genetics, 23(7), pp. 1802–1816. doi: 10.1093/hmg/ddt571.

Stenflo, J., Lundwall, A. and Dahlbäck, B. (1987) ‘β-Hydroxyasparagine in domains homologous to the epidermal growth factor precursor in vitamin K-dependent protein S.’, Proceedings of the National Academy of Sciences of the United States of America, 84(2), pp. 368–372. doi: 10.1073/pnas.84.2.368.

Stitt, T. N. et al. (1995) ‘The anticoagulation factor protein S and its relative, Gas6, are ligands for the Tyro 3/Axl family of receptor tyrosine kinases.’, Cell, 80(4), pp. 661–670. doi: 10.1016/0092-8674(95)90520-0.

Todt, J. C., Hu, B. and Curtis, J. L. (2004) 'The receptor tyrosine kinase MerTK activates phospholipase C gamma2 during recognition of apoptotic thymocytes by murine macrophages.', Journal of leukocyte biology, 75(4), pp. 705–713. doi: 10.1189/jlb.0903439.

Vajkoczy, P. et al. (2006) 'Dominant-negative inhibition of the Axl receptor tyrosine kinase suppresses brain tumor cell growth and invasion and prolongs survival.', Proceedings of the National Academy of Sciences of the United States of America, 103(15), pp. 5799–5804. doi: 10.1073/pnas.0510923103.

Valverde, P. (2005) 'Effects of Gas6 and hydrogen peroxide in Axl ubiquitination and downregulation', Biochem Biophys Res Commun., doi: 10.1016/j.bbrc.2005.05.086.

Varnum, B. C. et al. (1995) 'Axl receptor tyrosine kinase stimulated by the vitamin K-dependent protein encoded by growth-arrest-specific gene 6.', Nature, 373(6515), pp. 623–626. doi: 10.1038/373623a0.

Vouri, M. and Hafizi, S. (2017) 'TAM receptor tyrosine kinases in cancer drug resistance', Cancer Research, 77(11), pp. 2775–2778. doi: 10.1158/0008-5472.CAN-16-2675.

Wimmel, A. et al. (2001) 'Axl receptor tyrosine kinase expression in human lung cancer cell lines correlates with cellular adhesion.', European journal of cancer (Oxford, England : 1990), 37(17), pp. 2264–2274. doi: 10.1016/s0959-8049(01)00271-4.

Wu, Y.-M., Robinson, D. R. and Kung, H.-J. (2004) 'Signal pathways in up-regulation of chemokines by tyrosine kinase MER/NYK in prostate cancer cells.', Cancer research, 64(20), pp. 7311–7320. doi: 10.1158/0008-5472.CAN-04-0972.

Xing, M. et al. (2020) 'Snake Cathelicidin Derived Peptide Inhibits Zika Virus Infection', Frontiers in Microbiology, 11(August), pp. 1–11. doi: 10.3389/fmicb.2020.01871.

Yamagata, M., Sanes, J. R. and Weiner, J. A. (2003) 'Synaptic adhesion molecules', Current Opinion in Cell Biology, 15, pp. 621–632. doi: 10.1016/S0955-0674(03)00107-8.